FEATURE ARTICLE

T. Daniel Crawford

Ab initio calculation of molecular chiroptical properties

Abstract This review describes the first-principles calculation of chiroptical properties such as optical rotation, electronic and vibrational circular dichroism, and Raman optical activity. Recent years have witnessed a flurry of activity in this area, especially in the advancement of density-functional and coupled cluster methods, with two ultimate goals: the elucidation of the fundamental relationship between chiroptical properties and detailed molecular structure, and the development of a suite of computational tools for the assignment of the absolute configurations of chiral molecules. The underlying theory and the basic principles of such calculations are given for each property, and a number of representative applications are discussed.

1 Introduction

Chiral molecules are characterized by a unique three-dimensional handedness, and the resulting pairs of left- and right-handed enantiomers often exhibit distinct chemical activities when reacting within a chiral environment [1]. For example, there are literally dozens of examples of chiral species whose enantiomers produce dramatically differing odors, such as the naturally occurring limonene (**1**) (see Fig. 1): while one enantiomer smells of oranges, the odor of the other resembles turpentine [2]. A more serious example, however, is the drug thalidomide (**2**), which was prescribed to pregnant women in Europe between 1957 and 1962 for morning sickness. The drug was withdrawn soon thereafter when numerous cases of birth defects were reported, and later studies of rodent offspring indicated that one enantiomer of thalidomide was found to produce fetal-tissue damage while the other had no apparent effect. Unfortunately, both enantiomers are formed in vivo in humans through rapid interconversion, such that a non-racemic application of the two forms is not possible [3]. Although the FDA never approved the drug for use in the

U.S. in the 1960s, it did provide limited access to it beginning in 1998 for the treatment of erythema nodosum leprosum (ENL), a complication of Hansen's disease (leprosy).

Enantiomeric pairs of chiral molecules also exhibit distinct responses to left- and right-circularly polarized light in absorption, refraction, and scattering. These responses may be used to determine the handedness (i.e., the "absolute configuration") of an enantiomerically pure sample, provided sufficient details about the corresponding circular dichroism, birefringence, or scattering intensity differences are known a priori. Such analyses are vital to modern synthetic organic chemistry, for example, where the laboratory synthesis of chiral species such as natural product isolates requires careful control over the absolute and relative configurations of stereogenic centers. Although organic chemists routinely determine enantiomeric purity of such isolates by chiral chromatography (GC/HPLC), determination of the absolute configurations of non-crystalline compounds frequently requires asymmetric total synthesis, followed by comparison of the measured chiroptical responses to those of the initial isolate. If the given compound's structure allows for a large number of stereoisomers — and many natural products can give rise to literally thousands of such species — the synthesis of the desired enantiomer can require decades to complete.

Theory has an opportunity to play an important role in this effort. As ab initio quantum chemical methods have matured over the last several decades, so too has their ability to predict accurately, reliably, and rapidly a variety of molecular properties. Numerous examples have been reported in the literature for which theoretical data have preceded, confirmed, and even overturned experimental determinations of geometrical structure, vibrational and UV/Vis spectra, thermochemistry, NMR chemical shieldings, and spin–spin coupling constants [4–6]. In the last 10–15 years, tremendous advances have also been made in the extension of quantum chemical models to chiroptical properties, with the goal of developing computational methods for assisting in the determination of the absolute configurations of chiral species. Of equal importance, however, is a more fundamental objective: obtaining a deeper understanding of the very nature of optical activity. Although

T. D. Crawford
Department of Chemistry, Virginia Tech, Blacksburg, VA 24061, USA
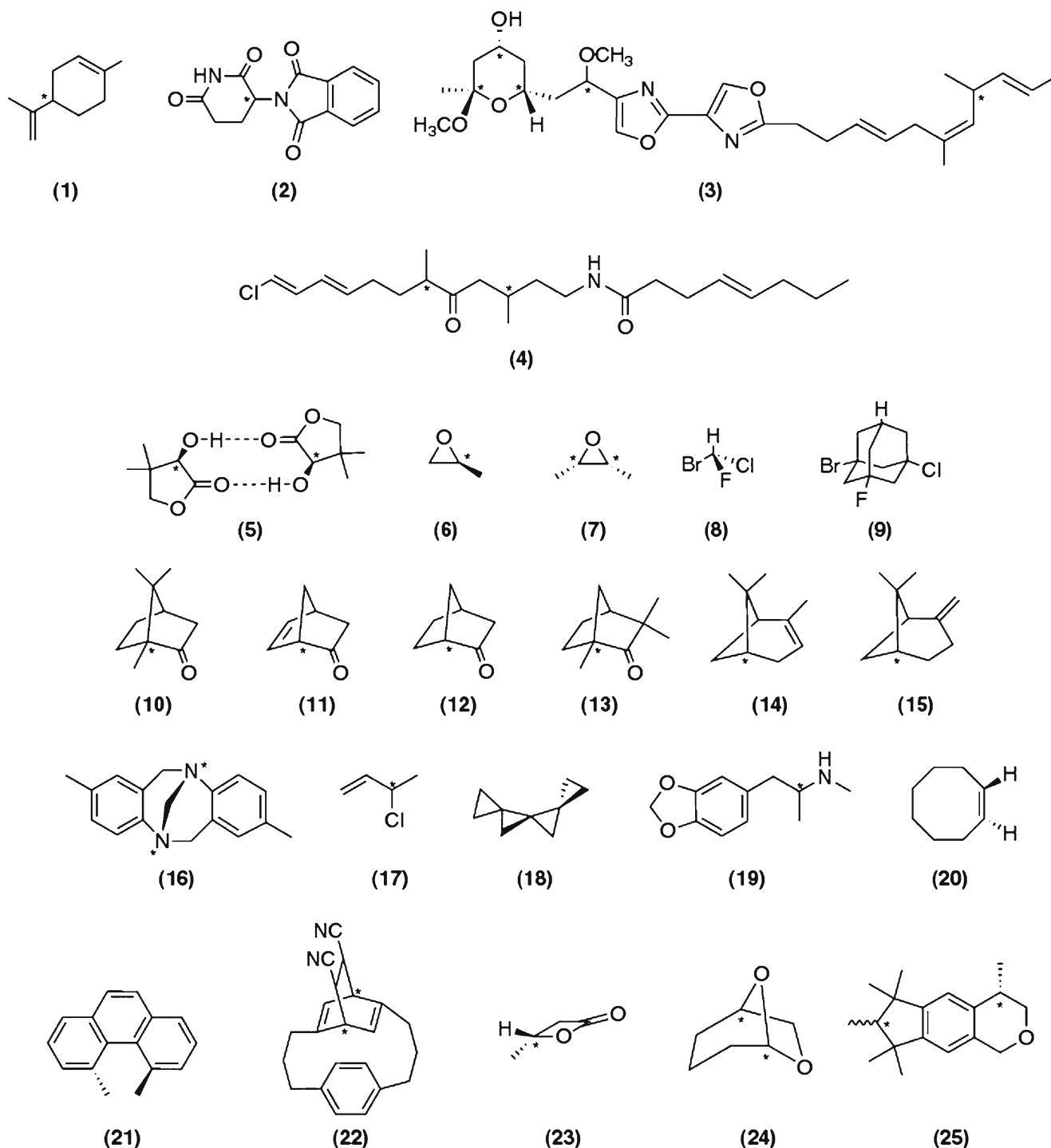E-mail: crawdad@vt.edu

Fig. 1 Chiral molecules discussed in this review. Stereogenic centers are indicated by *asterisks*, where applicable. Structures **18**, **20**, and **21** contain stereogenic axes, and structure **9** does not contain an atom at its stereogenic center

empirical rules such as the octant rule have been widely used by organic chemists for decades [7], they quickly fail outside the limited spectrum of simple molecules for which they were initially designed [8]. On the other hand, although advanced theoretical models can be used as a convenient black box, their value is greatly diminished if they do not also provide useful insight into the physical and chemical processes they represent [9]. Thus, much of the effort expended in modeling chiroptical properties has also focused on the inherent relationship of such properties to molecular structure and inter-/intra-molecular interactions.

This review summarizes the fundamental aspects of theoretical calculations of several types of chiroptical response properties that have been particularly valuable to organic and

biological chemistry: optical rotation, electronic and vibrational circular dichroism, and Raman optical activity. For each of these properties, we give a brief résumé of the underlying quantum mechanical principles, followed by a discussion of their implementation within state-of-the-art quantum chemical program packages and recent example applications.

We specifically focus on ab initio models, including Hartree-Fock and density-functional theory (DFT) [10], as well as the more recent advances in high-level electron-correlation methods, such as coupled cluster theory [11, 12]. These methods differ distinctly in their respective implementations, and each has its own advantages and disadvantages. DFT and its time-dependent variant (TD-DFT) have seen perhaps the widest application to chiroptical properties in the last several years, due to their effective balance of cost and accuracy. The scaling of DFT with molecular size is relatively low — comparable to its Hartree-Fock counterpart — and, thanks to state-of-the-art integral-direct techniques employed in several publicly available program packages, DFT calculations on chiral molecules containing 20–30 non-hydrogen atoms are now routine. In addition, compared to Hartree-Fock methods, which include essentially no electron correlation effects, modern hybrid functionals offer significantly improved accuracy, comparable or often superior to low-order perturbation theory methods such as MP2 [13, 14].

On the other hand, a drawback of DFT for chiroptical properties is their dependence on exchange-correlation functionals that were not designed for such calculations. For example, the popular "B3" exchange functional of Becke is considered by some to be "semi-empirical" in that its three parameters were obtained by a least-squares fit to experimental data (atomization energies, ionization potentials, proton affinities, and atomic energies) for the G2 test set of molecules [15]. Thus, while functionals such as B3LYP [15, 16] often do a superb job in thermochemical predictions, there is no fundamental physical reason for them to perform as admirably for more complicated properties such as optical rotation, where the response of the density is the pivotal quantity. Furthermore, fundamental deficiencies in even state-of-the-art functionals such as self-interaction errors, lack of dispersion effects, and qualitatively incorrect descriptions of diffuse electronic states are sometimes cause for skepticism regarding DFT results. New functionals currently under development may overcome such problems, but a truly universal functional remains out of reach.

Wave-function-based methods such as coupled cluster theory, on the other hand, are sometimes referred to as "convergent" models in the sense that one may extend the atomic orbital basis set and/or include higher levels of dynamic electron correlation to systematically approach the exact (Born–Oppenheimer) solution. This provides a natural set of diagnostics for the wave function that can lend greater confidence in the computed results. Unfortunately, the high-degree polynomial scaling of such methods [$\mathcal{O}(N^6)$ or worse] usually precludes their routine application to molecules containing more than 10–12 non-hydrogen atoms. This disadvantage is under attack, however, with the on-going development of reduced-scaling/locally-correlated coupled cluster methods [17–20], including new techniques that are applicable to chiroptical properties [21].

Although this review endeavors to provide an up-to-date perspective on modern ab initio methods for optical activity, it is far from comprehensive in its treatment of either the underlying theory or experimental techniques for measuring such properties. The indispensible text by Barron, "Molecular Light Scattering and Optical Activity" [22], the second edition of which has just been published, provides a much wider perspective on this topic. In addition, older texts by Caldwell and Eyring [23], Charney [24], and Mason [25] offer excellent pedagogical overviews of the fundamental theory. A number of excellent reviews focusing on specific classes of chiroptical properties have also appeared in recent years, including studies of optical rotation by Polavarapu [26] and by Stephens et al. [27, 28] reviews of vibrational circular dichroism by Polavarapu [29], by Stephens and Devlin [30], by Freedman et al. [31], and reviews of Raman optical activity calculations and measurements by Nafie [32] who also reviews VCD and by Barron et al. [33]. Furthermore, although we have chosen to limit our scope to natural (linear) optical activity, i.e. the optical response of chiral molecules to weak fields, we note that much effort has gone into theoretical descriptions of closely related magnetochiral [34–38] and non-linear [39] spectroscopic methods, such as the well-known techniques of magnetic circular dichroism [40, 41] and recently proposed chiral NMR [42].

2 Optical rotatory dispersion

Optical rotation (or circular birefringence) refers to the rotation of the plane of linearly polarized light as it passes through an enantiomerically pure sample of a chiral species. The magnitude of this rotation is characteristic of the detailed molecular structure of the compound and varies with the wavelength of the incident light (optical rotatory dispersion). This phenomenon was first observed by Arago in 1811 and by Biot in 1812 in quartz crystals, and Biot's later experiments established that the same rotation could be observed in solutions of camphor and turpentine. (For an excellent review of the historical development of optical activity as well as its fundamental quantum mechanical principles, see [22].) Optical rotation is now routinely measured in polarimetry experiments and has become an essential tool of organic chemistry.

The quantum mechanical foundations of optical rotation were first laid down more than 75 years ago by Rosenfeld [43], who demonstrated, using time-dependent perturbation theory, that the electric dipole moment of a chiral molecule induced by a frequency-dependent electromagnetic field may be written as [23]

$$\bar{\boldsymbol{\mu}} = \alpha \boldsymbol{E} + \beta \frac{\partial \boldsymbol{B}}{\partial t}, \tag{1}$$

where $\boldsymbol{E}$ and $\boldsymbol{B}$ represent the applied, time-dependent electric and magnetic field vectors. The α tensor denotes the usual

dipole-polarizability, e.g.,

$$\alpha_{xy}(\omega) = \frac{2}{\hbar} \sum_{n \neq 0} \frac{\omega_{n0} \langle \psi_0 | \mu_x | \psi_n \rangle \langle \psi_n | \mu_y | \psi_0 \rangle}{\omega_{n0}^2 - \omega^2}, \tag{2}$$

where $\boldsymbol{\mu} = \sum_i q_i \boldsymbol{r}_i$ is the electric-dipole operator, ω is the frequency of the incident radiation field, ψ_0 denotes the ground-state wave function, and the summation runs over all electronically excited states, ψ_n, each with excitation energy, ω_{n0}. The key quantity developed by Rosenfeld is the analogous β tensor,

$$\beta_{xy}(\omega) = -\frac{2}{\hbar} \text{Im} \sum_{n \neq 0} \frac{\omega \langle \psi_0 | \mu_x | \psi_n \rangle \langle \psi_n | m_y | \psi_0 \rangle}{\omega_{n0}^2 - \omega^2}, \tag{3}$$

where $\boldsymbol{m} = \sum_i \frac{q_i}{2m_i} \boldsymbol{r}_i \times \boldsymbol{p}_i$ is the magnetic dipole operator and "Im" indicates that only the imaginary part of the expression is retained.

The trace of β is related to the *specific rotation* [i.e., the total rotation, normalized for path length (dm) and concentration (g/mL)], which is commonly denoted as $[\alpha]_\omega$. Averaging over all molecular orientations [23] (followed by considerable algebraic manipulation) leads to the following expression for $[\alpha]_\omega$, in $\deg \, \text{dm}^{-1} \, (\text{g/mL})^{-1}$:

$$[\alpha]_\omega = \frac{(72.0 \times 10^6) \, \hbar^2 N_A \omega}{c^2 m_e^2 M} \times \left[\frac{1}{3} \text{Tr}(\beta) \right] \tag{4}$$

where β and ω are given in atomic units, N_A is Avogadro's number, c is the speed of light (m/s), m_e is the electron rest mass (kg), and M is the molecular mass (amu).

Although the Rosenfeld expression for β in Eq. 3 involves summation over the molecular excited states, most quantum chemical calculations of $[\alpha]_\omega$ avoid this approach in practice by invoking a linear response formalism [44,45],

$$\beta_{xy}(\omega) = -\text{Im} \langle \langle \mu_x; m_y \rangle \rangle_\omega, \tag{5}$$

in which the perturbation of the ground-state wave function by the external electric and magnetic fields is the central quantity. This approach generally requires relatively straightforward solution of systems of coupled linear equations for the perturbed wave functions, followed by direct calculation of β.

2.1 Hartree-Fock and DFT optical rotation calculations

In Hartree-Fock and DFT approaches, the frequency dependence of the applied field implies the need for a time-dependent formalism — time-dependent Hartree-Fock (TD-HF) or the random phase approximation (RPA) [46,44] for the former, and time-dependent DFT (TD-DFT) for the latter [47, 48]. In these approaches, the response function for $\beta_{xy}(\omega)$ may be written as

$$\langle \langle \mu_x; m_y \rangle \rangle_\omega = \boldsymbol{\mu}_x^+ (\boldsymbol{\Gamma} - \omega \boldsymbol{\Delta})^{-1} \boldsymbol{m}_y, \tag{6}$$

where $\boldsymbol{\mu}_x$ and $\boldsymbol{m}_y$ denote vectors of the electric-dipole and magnetic-dipole operator components, respectively,

$$\boldsymbol{\Gamma} = \begin{pmatrix} \boldsymbol{A} & \boldsymbol{B} \\ \boldsymbol{B} & \boldsymbol{A} \end{pmatrix} \tag{7}$$

and

$$\boldsymbol{\Delta} = \begin{pmatrix} \boldsymbol{1} & \boldsymbol{0} \\ \boldsymbol{0} & -\boldsymbol{1} \end{pmatrix}, \tag{8}$$

and the implied matrix dimensions include all single excitations and de-excitations among the Hartree-Fock or Kohn-Sham molecular orbitals. The elements of the submatrices $\boldsymbol{A}$ and $\boldsymbol{B}$ are

$$A_{aibj} = (\epsilon_a - \epsilon_i) \delta_{ij} \delta_{ab} + \langle aj || ib \rangle \tag{9}$$

and

$$B_{aibj} = \langle ab || ij \rangle, \tag{10}$$

where i and j (a and b) denote occupied (virtual) molecular orbitals, ϵ_i and ϵ_a are orbital energies, and $\langle pq || rs \rangle$ is an antisymmetrized electron repulsion integral in Dirac's notation. In the TD-DFT approach, the two-electron integrals naturally include contributions from the exchange-correlation potential employed [49–52]. In practice, the matrix inverse appearing in Eq. 6 is not computed explicitly, but instead a system of linear equations is defined for the associated right-hand perturbed wave function, e.g.,

$$(\boldsymbol{\Gamma} - \omega \boldsymbol{\Delta}) \, \boldsymbol{Z}_x = \boldsymbol{\mu}_x. \tag{11}$$

This equation may be simplified for computations by expanding the super-matrix expression into a pair of reduced-dimension matrix equations using $\boldsymbol{A}$ and $\boldsymbol{B}$ explicitly [44]. Thus, a computation of the linear response function for Hartree-Fock or DFT requires the following steps:

1. Solution of the SCF equations to obtain the initial HF or KS molecular orbitals.
2. Construction of the $\boldsymbol{A}$ and $\boldsymbol{B}$ matrices using the appropriate forms of Eqs. 9 and 10. (This may be carried out in an integral-direct manner, for example.)
3. Iterative solution of Eq. 11 for each Cartesian component of $\hat{\boldsymbol{\mu}}$ (or $\hat{\boldsymbol{m}}$) — a total of three perturbed wave function equations.

The final tensor element is obtained by taking dot products of $\boldsymbol{Z}_\alpha$ with $\boldsymbol{m}_\beta$. The cost of such a calculation is comparable to the solution of the coupled-perturbed Hartree-Fock or Kohn-Sham equations required for a normal coordinate analysis.

The first Hartree-Fock calculations of optical rotation were reported by Polavarapu in 1997 [53] using the "static-limit" Rosenfeld tensor program developed in CADPAC by Amos [54]. Two years later, the first density-functional-based optical rotation calculations were reported in 1999 by Yabana and Bertsch within the local density approximation (LDA). Cheeseman, Frisch, Devlin, and Stephens reported static-limit DFT calculations of optical rotation in 2000 using hybrid functionals such as B3LYP [55], and in 2001 they extended this work to include frequency dependence [56].

Several ab initio program packages now include optical rotation calculations at the Hartree-Fock level [57–61], and density-functional implementations, using both pure functionals and hybrid Hartree-Fock exchange, are now publicly available as well [58,59,62,61]. The most efficient implementations of these models make use of integral direct

techniques, in which the required two-electron integrals are computed "on-the-fly" rather than precomputed and stored, as well as "resolution of the identity" (RI) methods (for pure functionals), in which certain classes of integrals are approximated as products of integrals that are less expensive to compute [63]. Both the direct and RI approaches make possible applications of TD-HF and TD-DFT optical rotations for molecules containing up to several dozen non-hydrgen atoms by reducing the disk-space and CPU-time requirements of such calculations.

2.2 Coupled cluster optical rotation calculations

One of the most reliable quantum chemical approaches for many molecular properties is coupled cluster theory [11, 12], a size-extensive model in which the electronic wave function is constructed as an exponential expansion of Slater determinants, viz.

$$|\psi_{\mathrm{CC}}\rangle = \mathrm{e}^{\hat{T}}|\psi_0\rangle, \tag{12}$$

where $\hat{T}$ is a "cluster operator", which formally generates excited/substituted determinants from the reference determinant, ψ_0 (usually, but not necessarily a Hartree-Fock wave function). The cluster operator must be truncated at a selected level of excitation for practical calculations, e.g. the coupled cluster singles and doubles (CCSD) approach is defined as limiting $\hat{T}$ to include only singly and doubly excited determinants. The advantage of the exponential form of the wave function is that the power-series expansion of $\exp(\hat{T})$ implicitly includes higher excitations beyond those for which $\hat{T}$ is truncated, and the total wave function for non-interacting systems may be written as a product of the wave functions for the fragments. The coupled cluster energy is, however, non-variational, because it is determined as the reference expectation value of a non-hermitian, similarity-transformed Hamiltonian, $\bar{H}$:

$$E_{\mathrm{CC}} = \langle\psi_0|\mathrm{e}^{-\hat{T}}\hat{H}\mathrm{e}^{\hat{T}}|\psi_0\rangle = \langle\psi_0|\bar{H}|\psi_0\rangle. \tag{13}$$

This leads to distinct right- and left-hand wave functions:

$$\langle\tilde{\psi}_{\mathrm{CC}}| = \langle\psi_0|\left(1 + \hat{\Lambda}\right)\mathrm{e}^{-\hat{T}}, \tag{14}$$

where $\hat{\Lambda}$ is a de-excitation cluster operator, analogous to $\hat{T}$.

A coupled cluster implementation of the Rosenfeld tensor requires a time-dependent response approach, similar in foundation to that of the TD-HF and TD-DFT methods described above, but which must take into account the response of both the left- and right-hand coupled cluster wave functions [64–66]. This leads to the following second-quantized expression for the linear response function:

$$\langle\langle\boldsymbol{\mu}; \mathbf{m}\rangle\rangle_\omega = \frac{1}{2}\hat{C}^{\pm\omega}\left[\langle\psi_0|\hat{\Lambda}\left[\bar{\boldsymbol{\mu}}, \hat{X}_{\mathbf{m}}^\omega\right]|\psi_0\rangle \right.$$
$$\left. + \langle\psi_0|\left[\hat{Y}_{\mathbf{m}}^\omega, \bar{\boldsymbol{\mu}}\right]|\psi_0\rangle\right], \tag{15}$$

where the overbar denotes similarity transformation of the given operator [just as for the Hamiltonian in Eq. 13], and

the permutation operator $\hat{C}^{\pm\omega}$ simultaneously changes the signs on the chosen field frequency and takes the complex conjugate of the expression. The perturbed $\hat{T}$ and $\hat{\Lambda}$ cluster operators, which are given by $\hat{X}_{\mathbf{m}}^\omega$ and $\hat{Y}_{\mathbf{m}}^\omega$, respectively, are computed by solving systems of linear equation, analogous to Eq. 11, e.g.,

$$\sum_j \langle\psi_i|(\bar{H} - \omega)|\psi_j\rangle\langle\psi_j|\hat{X}_{\mathbf{m}}^\omega|\psi_0\rangle = -\langle\psi_i|\bar{\mathbf{m}}|\psi_0\rangle, \tag{16}$$

and

$$\sum_j \langle\psi_0|\hat{Y}_{\mathbf{m}}^\omega|\psi_j\rangle\langle\psi_j|(\bar{H} + \omega)|\psi_i\rangle$$
$$= -\langle\psi_0|\hat{\Lambda}\left[\bar{\mathbf{m}}, \hat{\tau}_i\right]|\psi_0\rangle$$
$$- \langle\psi_0|\hat{\Lambda}\left[\left[\bar{H}, \hat{X}_{\mathbf{m}}^\omega\right], \hat{\tau}_i\right]|\psi_0\rangle, \tag{17}$$

where $\hat{\tau}_i$ represents an excitation operator that produces the i-th excited Slater determinant from the reference ψ_0. An alternative expression for the linear response function may be obtained by making use of the dependence of $\hat{Y}_{\mathbf{m}}^\omega$ on $\hat{X}_{\mathbf{m}}^\omega$ to obtain

$$\langle\langle\boldsymbol{\mu}; \mathbf{m}\rangle\rangle_\omega = \frac{1}{2}\hat{C}^{\pm\omega}\hat{P}\left(\boldsymbol{\mu}(-\omega), \mathbf{m}(\omega)\right)$$
$$\times \left[\langle\psi_0|\hat{\Lambda}\left[\bar{\boldsymbol{\mu}}, \hat{X}_{\mathbf{m}}^\omega\right]|\psi_0\rangle \right.$$
$$\left. + \frac{1}{2}\langle\psi_0|\hat{\Lambda}\left[\left[\bar{H}, \hat{X}_{\boldsymbol{\mu}}^\omega\right], \hat{X}_{\mathbf{m}}^{-\omega}\right]|\psi_0\rangle\right], \tag{18}$$

where $\hat{P}$ is a symmetric permutation operator. Thus, a computation of the coupled cluster linear response function for two different operators, $\hat{\boldsymbol{\mu}}$ and $\hat{\mathbf{m}}$, requires the following steps:

1. Solution of the ground-state coupled cluster $\hat{T}$ and $\hat{\Lambda}$ amplitude equations. (These quantities are also required for analytic energy gradients, for example.)
2. Solution of the perturbed wave functions, $\hat{X}_{\mathbf{m}}^\omega$ and $\hat{X}_{\boldsymbol{\mu}}^\omega$, in Eq. 16 for each Cartesian component of the operators at both positive and negative field frequencies — a total of 12 sets of linear equations.
3. Construction of the linear response function in Eq. 18 using $\hat{T}$, $\hat{\Lambda}$, and the perturbed wave functions.

The overall cost of a coupled cluster linear response calculation is similar to that for NMR chemical shieldings, for example. However, the need to solve for 12 perturbed wave functions for each field frequency makes calculations of optical rotatory dispersion (ORD) particularly expensive.

Ruud et al. [50, 67] reported the first CCSD level calculations in the DALTON package [68] in 2002, and Crawford et al. [69, 70] recently implemented coupled cluster optical rotation in the PSI3 package [60]. Most recently, Pedersen et al. [71]. have reported the first application of optical rotation at the CC3 level of theory, which includes connected triple excitations [72], again using a developmental version of the DALTON package.

2.3 Origin invariance

One subtle problem arising in calculations of the Rosenfeld β tensor is that of origin dependence: in the formalism given above for Hartree-Fock, DFT, and coupled cluster, a translation of the coordinate origin along a vector, $\mathbf{a}$, leads to a shift in the computed value of $[\alpha]_\omega$, clearly an unphysical result. This problem can be understood in terms of the response functions above by first noting that the origin shift changes the coordinate, linear momentum, and angular momentum vectors as $\mathbf{r}' = \mathbf{r} - \mathbf{a}$, $\mathbf{p}' = \mathbf{p}$, and $\mathbf{r}' \times \mathbf{p}' = \mathbf{r} \times \mathbf{p} - \mathbf{a} \times \mathbf{p}$, respectively. The corresponding linear-response tensor at the new origin may then be written as,

$$\langle\langle \mathbf{r}'; \mathbf{r}' \times \mathbf{p}' \rangle\rangle_\omega = \langle\langle \mathbf{r}; \mathbf{r} \times \mathbf{p} \rangle\rangle_\omega - \langle\langle \mathbf{r}; \mathbf{a} \times \mathbf{p} \rangle\rangle_\omega. \tag{19}$$

The trace of the second term on the right-hand side of the equation, which is the source of the origin dependence, may be written explcitly in terms of the individual components of $\mathbf{r}$, $\mathbf{p}$, and $\mathbf{a}$ as,

$$\begin{aligned}
\mathrm{Tr}\langle\langle \mathbf{r}; \mathbf{a} \times \mathbf{p} \rangle\rangle_\omega = {}& a_x \left[\langle\langle r_z; p_y \rangle\rangle_\omega - \langle\langle r_y; p_z \rangle\rangle_\omega \right] \\
& + a_y \left[\langle\langle r_x; p_z \rangle\rangle_\omega - \langle\langle r_z; p_x \rangle\rangle_\omega \right] \\
& + a_z \left[\langle\langle r_y; p_x \rangle\rangle_\omega - \langle\langle r_x; p_y \rangle\rangle_\omega \right].
\end{aligned} \tag{20}$$

Thus, the variation of the optical rotation with a change of origin is dependent on both the size of the shift and the asymmetry of the $\langle\langle \mathbf{r}; \mathbf{p} \rangle\rangle_\omega$ response function. If, however, the electronic structure model used to compute $\langle\langle \mathbf{r}; \mathbf{p} \rangle\rangle_\omega$ satisfies the correponding equation-of-motion of the response function [44],

$$\omega\langle\langle \mathbf{r}; \mathbf{r} \rangle\rangle_\omega = \langle \psi_0 |[\mathbf{r}, \mathbf{r}]| \psi_0 \rangle + \langle\langle \mathbf{r}; [\mathbf{r}, \hat{H}] \rangle\rangle_\omega, \tag{21}$$

then the optical rotation becomes origin invariant in the limit of a complete basis set because then

$$[\mathbf{r}, \hat{H}] = i\mathbf{p}. \tag{22}$$

In this case, $\langle\langle \mathbf{r}; \mathbf{p} \rangle\rangle_\omega$ may be replaced with $\omega\langle\langle \mathbf{r}; \mathbf{r} \rangle\rangle_\omega$ in Eq. 20, which becomes zero due to the symmetry of the latter. This is the case for Hartree-Fock and DFT, whose response functions satisfy Eq. 21, but not for coupled cluster theory [66, 73].

For practical basis sets, one approach to overcoming the origin-dependence problem is to incorporate directly into the basis functions a magnetic-field-dependent phase factor, leading to what are known as gauge-including atomic orbitals (GIAOs) or London atomic orbitals (LAO's), defined as [74, 75]

$$\chi_\nu(\mathbf{B}; \mathbf{R}_\nu; \mathbf{r}) = \exp\left(-\frac{i}{2}(\mathbf{B} \times \mathbf{R}_\nu) \cdot \mathbf{r} \right) \chi(0; \mathbf{R}_\nu; \mathbf{r}), \tag{23}$$

where $\mathbf{R}_\nu$ is the coordinate of the nucleus on which the ν-th basis function resides and $\chi(0; \mathbf{R}_\nu; \mathbf{r})$ is the original (Gaussian) basis function. GIAOs have seen wide application in quantum chemistry in the last 10–15 years, especially in the calculation of NMR chemical shieldings, where comparable issues of origin invariance arise [76–78]. When GIAOs are employed, the response function $\langle\langle \mathbf{r}; \mathbf{p} \rangle\rangle_\omega$ appearing

in Eq. 20 is replaced naturally by $\langle\langle \mathbf{r}; [\mathbf{r}, H] \rangle\rangle_\omega$, which, by Eq. 21, is equal to $\omega\langle\langle \mathbf{r}; \mathbf{r} \rangle\rangle_\omega$ [79, 80]. Again, the symmetry of the latter function forces Eq. 20 to zero, thus ensuring origin invariance of the optical rotation, even for finite basis sets. GIAO-based Hartree-Fock and DFT optical rotation techniques are available in several program packages [58, 68].

The fact that Eq. 21 does not hold for methods like coupled cluster theory [66, 81] implies that GIAOs will not ensure origin invariance, even in the limit of a complete basis set. However, as used recently by Grimme et al. [63] and by Pedersen et al. [82] an alternative representation of the Rosenfeld tensor may be employed to circumvent this problem. For exact wave functions,

$$\mathrm{Tr}\langle\langle \mathbf{r}; \mathbf{r} \times \mathbf{p} \rangle\rangle_\omega = \frac{1}{\omega}\mathrm{Tr}\langle\langle \mathbf{p}; \mathbf{r} \times \mathbf{p} \rangle\rangle_\omega, \tag{24}$$

according to Eq. 21. The trace on the right-hand side of this equation is inherently origin independent because, if the origin-shifted equivalent expression for Eq. 19 were constructed, the symmetric response function $\langle\langle \mathbf{p}; \mathbf{p} \rangle\rangle_\omega$ would appear, forcing Eq. 20 to zero. However, a fundamental problem with this "velocity-gauge" representation of the response function within coupled cluster theory is that it does not decay to zero in the static limit as does its "length-gauge" counterpart because of the appearance of $1/\omega$ in Eq. 24, which cancels the ω in the numerator of Eq. 4. Thus, Pedersen et al. recommended shifting $\langle\langle \mathbf{p}; \mathbf{r} \times \mathbf{p} \rangle\rangle_\omega$ by its static-limit value, $\langle\langle \mathbf{p}; \mathbf{r} \times \mathbf{p} \rangle\rangle_0$ to account for this error. Although this requires the solution of an additional set of six perturbed wave function equations (for a total of 18), the result is a well-behaved, origin-invariant expression for the optical rotation that applies equally well to DFT and coupled cluster theory. We note, however, that the origin invariance of the velocity-gauge expression applies only to the *trace* of the corresponding Rosenfeld tensor, not its individual components, and, again, even in the limit of a complete basis set, the velocity- and length-gauge expressions for the Rosenfeld tensor will not give equivalent results within the truncated coupled cluster approximation [66, 81].

2.4 Applications

The last decade has witnessed tremendous activity in theoretical calculations of optical rotation, and we describe here a number of particularly relevant results. For an excellent and more complete review of recent optical rotation calculations, as well as a discussion of both semiempirical and quantum mechanical techniques, see Polavarapu [26] and Stephens et al. [27, 28].

The first systematic study of optical rotation by ab initio methods was carried out in 1997 by Polavarapu using Hartree-Fock theory with small basis sets for the "static-limit" Rosenfeld tensor (defined as the overlap of wave function derivatives with respect to external electric and magnetic fields [54]) without London orbitals [53, 83, 84]. At around the same time, Kondru, Wipf, and Beratan applied this same

approach to a number of natural products [85, 86], making use of van't Hoff's superposition principle that the total specific rotation of a large molecule may be estimated as the sum of the rotations of its component fragments. Using GIAO-based Hartree-Fock 6-31G calculations, they determined the optical rotation of the natural product hennoxazole A (**3**) [85]. They divided the system into three subsystems of comparable size, optimized the lowest-lying conformers of each stereoisomer using a molecular mechanics approach (including $CHCl_3$ solvent corrections), and Boltzmann-averaged the computed optical rotations. The final estimated rotations agreed well in both sign and magnitude with the measured rotations for each of eight stereoisomers, and the best match with the measured $[\alpha]_{589}$ of the original natural product agreed with an earlier assignment using asymmetric total synthesis. Ribe et al. [87] carried out a comparable analysis for the marine natural product pitiamide A (**4**) 2 years later However, Goldsmith et al. [88] recently reported a failure of van't Hoff's superposition principle when applied to molecular aggregates. Using DFT/B3LYP calculations of $[\alpha]_{589}$ for conformationally averaged monomeric and dimeric (R)-$(-)$-pantolactone (**5**), they predicted a value of $[\alpha]_{589}$ for the monomer of only -1 deg dm^{-1} (g/mL)$^{-1}$ and for the dimer of -203 deg dm^{-1} (g/mL)$^{-1}$.

We also note the effort by Kondru, Wipf, and Beratan to establish a foundation for the long-elusive structure-property relationships of optical rotation. They proposed [89] a Mulliken-like partitioning of the "static" optical rotation tensor into atomic contributions [54]. This allows the visual interpretation of each atom's contribution to the total rotation.

In 2000, Cheeseman et al. [55] reported the first DFT calculations of the static-limit optical rotation using GIAOs. They applied this new technique to (S)-methyloxirane (**6**) and (R,R)-dimethyloxirane (**7**) with a variety of large basis sets, with and without diffuse functions and with polarization functions up to g-type. They concluded that small basis sets do not provide reliable results. A year later, they extended this effort to include frequency dependence. In a systematic analysis of 30 molecules with several basis sets, they found that Hartree-Fock level optical rotations were generally not reliable and gave much larger average absolute errors compared to experiment — by a factor of three — as compared to B3LYP rotations. In addition, they found that the inclusion of a simple Lorenz solvent correction reduced the accuracy of the calculations [56]. Several additional applications making use of DFT for assignment of absolute configuration have recently been reported [90, 27, 28].

Polavarapu used multi-wavelength Hartree-Fock and DFT/ B3LYP calculations of optical rotation for the paradigmatic chiral molecule (S)-bromochlorofluoromethane (**8**) [91] using London orbitals and large basis sets for comparison with earlier Raman optical activity analyses of its absolute configuration [92]. He reported that the computed ORD in the range of 589–365 nm compared well with the experimentally determined curve for the (+) enantiomer [91]. Schreiner et al. [93] synthesized an enantiomerically pure adamantane analogue of bromochlorofluoromethane (**9**) — a pseudotetrahe-

dral structure that is fascinating in part because it contains no atom at its stereogenic center. They succesfully assigned its absolute configuration based on a combination of theoretical predictions and experimental measurements.

Giorgio et al. [94] have recently recommended the use of multi-wavelength Hartree-Fock- and DFT-level optical rotation calculations, comparable to that used by Polavarapu above, a means to determine the absolute configurations of chiral species. They argue that, although such methods may give significant errors relative to experiment at a single wavelength, they will correctly reproduce the overall shape of the Cotton effect in regions far from an absorption pole. They demonstrated the usefulness of this approach for several molecules, including camphor (**10**), β-pinene (**15**), and Troger's base (**16**), among others.

However, this approach of computing ORD curves for comparison to experiment fails when the chosen field frequency, ω, approaches an excitation energy of the molecule, which case the expression for the Rosenfeld tensor given in Eq. 3 diverges, leading to a first-order pole structure in $[\alpha]_\omega$ (the Cotton effect [24]). This, however, is a breakdown of the underlying perturbation theory used to derive β, and, of course, experimental measurements of $[\alpha]$ in absorbing regions give only finite values. Norman et al. [95] recently addressed this problem by introducing an empirical factor into β to account for the finite lifetimes of the excited states. This allowed them to carry out the first calculations of the complete ORD curves for a number of systems using origin-invariant DFT calculations. Ultimately, a complete theoretical prediction of ORD curves using the approach of Norman et al. will require direct calculation of excited-state lifetimes.

Although conformational effects have been considered by many of the above studies, the first systematic investigations of the impact of structural flexibility have been reported by Wiberg and co-workers. In particular, they have investigated conformational averaging of optical rotation using DFT-level calculations for a number of prototypical systems, including substituted and unsubstituted butenes and butanes [96–98]. For 3-chloro-1-butene (**17**), for example, which has three important low-lying conformers that differ primarily in the C=C−C−C dihedral angle, they reported dramatic differences in $[\alpha]_{589}$, as determined by B3LYP calculations using GIAOs [96]. They were able to compute a Boltzmann average of the rotations for each conformer using G2- and G3-level free energies, but the final value of the rotation was still a factor of two larger than the experimental value. For 3-chlorobutane, however, which differs from its 1-butene counterpart only in its lack of a long wavelength $\pi \rightarrow \pi^*$ excitation, they obtained good agreement with experiment using the same approach [98]. In addition, Wiberg and co-workers investigated the effect of the choice of basis set on optical rotation using 30° twisted ethane as a test case. They found that diffuse p-type functions on hydrogen atoms were essential to correct descriptions of optical rotation, and that the 6-311++G** split-valence basis sometimes failed due to a lack of such functions [97].

The impact of the solvent on optical rotation is well known to be considerable for many systems, sometimes even changing the sign of the observed rotation for a given wavelength [99]. This problem has recently been addressed by Stephens and co-workers and by Mennucci et al. [100] using the polarizable continuum model (PCM) in conjunction with density functional calculations to determine shifts in $[\alpha]_{589}$ among several solvents. Stephens et al. focused on 6,8-bicyclo[3.2.1]octane derivatives and reported a reduction of about 4 $\deg \mathrm{dm}^{-1}$ $(\mathrm{g/mL})^{-1}$ (out of ca. 15 $\deg \mathrm{dm}^{-1}$ $(\mathrm{g/mL})^{-1}$) in the mean absolute deviation from experiment when solvent effects were included in the model. Mennucci et al. considered a test set of seven rigid chiral molecules, including α- (**14**) and β-pinene (**15**), camphor (**10**), and others, in both polar and non-polar solvents. They found that inclusion of electrostatic effects in the model were sufficient to correctly describe optical rotation in several solvents, such as cyclohexane, acetone, methanol, and acetonitrile, while for CCl_4, benzene, and chloroform, this approach was insufficient.

In 2002, Ruud and Helgaker [50] reported the first coupled-cluster calculations of optical rotation. Using CCSD-level response theory, they reported $[\alpha]_{589}$ values for hydrogen peroxide as a function of the $H-O-O-H$ dihedral angle, demonstrating its substantial dependence on the molecular conformation. The following year, Ruud et al. [67] reported a more systematic study of 15 molecules at the CCSD and CC2 [101] levels of theory and found that, for nearly all of the molecules considered, B3LYP and CCSD optical rotations performed equally well. The only exception was the larger molecule, (*1S,4S*)-(−)-norbornenone (**11**), for which CCSD was found to underestimate the experimental value of −1,146 $\deg \mathrm{dm}^{-1}$ $(\mathrm{g/mL})^{-1}$ by more than 35%. B3LYP, on the other hand, overestimated the experimental result by only 6%. The underlying reason for this discrepancy has yet to be determined.

In 2004, Tam et al. [69] reported an independent implementation of CCSD-level optical rotation and recently applied this technique [70], using the origin-independent, velocity-gauge approach of Pedersen et al. [82] to the σ-helicene, (*P*)-(+)-[4]triangulane (trispiro[2.0.0.2.1.1] nonane) (**18**), a rigid helical structure consisting of four fused cyclopropane rings. This molecule was synthesized in enantiomerically pure form in 1999 by de Meijere et al. [102,103] who also measured very large specific rotations — ranging from 192.6 $\deg \mathrm{dm}^{-1}$ $(\mathrm{g/mL})^{1}$ at 589 nm to more than 600 $\deg \mathrm{dm}^{-1}(\mathrm{g/mL})^{1}$ at 365 nm — even though the molecule contains no long-wavelength chromophore (see Fig. 2). CCSD optical rotations were found to compare superbly (to an average of only 1%) with the experimental results across the entire measured ORD curve. B3LYP and CC2 calculations produced qualitatively correct results, but both overestimated the rotations (by up to 16% for DFT and 8% for CC2). However, these results are not necessarily representative and, indeed, may be somewhat providential given that factors such as solvation, temperature, and zero-point vibration have not been accounted for.

The largest coupled cluster optical rotation calculations to date were reported by Pedersen et al. [82] at the CC2 level of theory on 3,4-methylenedioxymethamphetamine (MDMA, also known as the drug "ecstasy", **19**), which contains 29 atoms (14 non-hydrogen). These large-scale calculations were facilitated by a Cholesky integral decomposition technique in which the two-electron integrals, which are vast in number for large molecules, are approximated as products of a small number of small-dimension vectors [104,105]. This leads to considerable savings in the computation time (ca. a factor of ten) of response properties such as optical rotation.

In spite of these advances, it is not yet understood what level of theory is necessary to obtain "the right answer for the right reason" for optical rotation, and many of the above successes rely implicitly on fortuitous cancellation of errors (e.g., limited basis sets, lack of explicit solvation, vibrational averaging, etc.) This point is well illustrated by methyloxirane (also known as propylene oxide, **6**). Owing to its small size, this molecule is an ideal test case for ab initio models of optical rotation, and it has proved a substantial challenge. Vaccaro and co-workers recently carried out the first quantitative *gas-phase* measurements of optical rotation using their newly developed technique of cavity ring-down polarimetry (CRDP) [106,107], For (*S*)-methyloxirane, they measured a value of $[\alpha]$ at 355 nm to be +10.2 $\deg \mathrm{dm}^{-1}$ $(\mathrm{g/mL})^{-1}$, significantly different than the value reported by Kumata et al. at 589 nm of −18.7 $\deg \mathrm{dm}^{-1}$ $(\mathrm{g/mL})^{-1}$ in CCl_4 (Fig. 3).

Although recent studies show that, with appropriate basis sets, B3LYP optical rotations for methyloxirane agree reasonably well with both experimental values of $[\alpha]_{355}$ and $[\alpha]_{589}$ [69,108], coupled cluster methods fail to produce a positive rotation at 355 nm, regardless of basis set [69]. Although one might be tempted to conclude that DFT provides superior results for this system, the agreement between DFT and experiment is likely to be fortuitous in this case. In particular, Tam, Russ, and Crawford have shown that, unlike coupled cluster methods, which reproduce the lowest-lying excitation energy of methyloxirane of 7.15 eV (174.1 nm) to within 0.05 eV, B3LYP methods underestimate this value by 0.5–0.6 eV, a result typical of TD-DFT for diffuse Rydberg states [69]. As a result, B3LYP predicts a much earlier onset of the corresponding Cotton pole in the optical rotation (cf. Eq. 3) than CCSD, leading to positive rotations at longer wavelengths than if DFT reproduced the excitation energy correctly. On the other hand, the disagreement between coupled cluster optical rotations and experiment persist, even when triple excitations are included in the ansatz [71]. A possible explanation for the discrepancy between theory and experiment was recently offered by Ruud and Zanasi [109] who found that zero-point vibrational motion [110] (estimated at the B3LYP level of theory) led to a positive shift of 48.1 $\deg \mathrm{dm}^{-1}$ $(\mathrm{g/mL})^{-1}$ at 355 nm [109]. Such results beg the question of the general importance of vibrational effects for obtaining the right answer for the right reason, and only continued systematic studies will answer it.
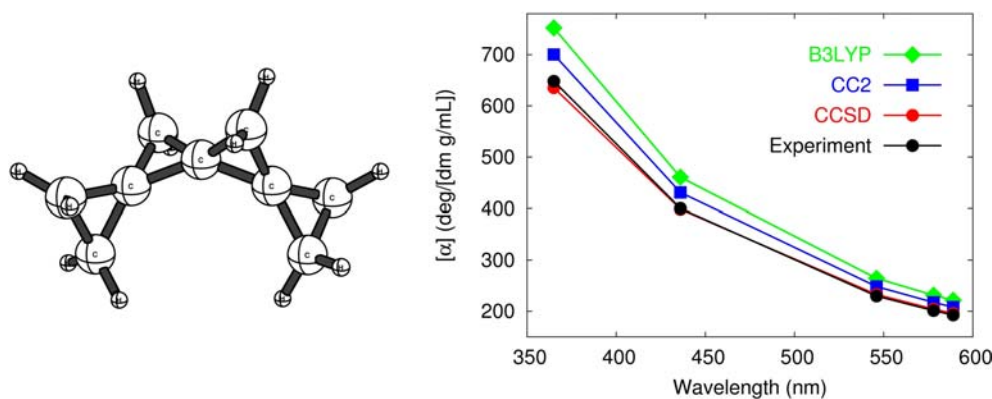
Fig. 2 Theoretical (B3LYP, CC2, and CCSD with the aug-cc-pVDZ basis set) and experimental optical rotatory dispersion curves for (*P*)-(+)-[4]triangulane (**18**). The aug-cc-pVDZ basis set was used for the theoretical curves. Theoretical data were taken from Ref. [70] and experimental data from Ref. [102]
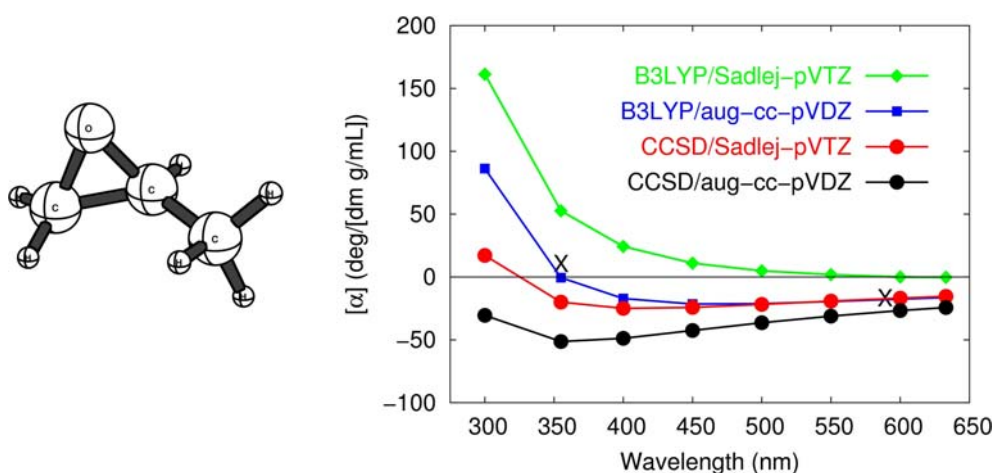

Fig. 3 Theoretical optical rotatory dispersion curves for (*S*)-methyloxirane (shown on the left). The positions marked with an "X" are the measured experimental rotations in the gas-phase (+10.2 deg dm^{-1} (g/mL)$^{-1}$, 355 nm, [106]) and in solvent (CCl$_4$, −18.7 deg dm^{-1} (g/mL)$^{-1}$, 589 nm, [99]). Theoretical data were taken from Ref. [69]

3 Electronic circular dichroism spectra

Electronic circular dichroism (ECD) spectra are derived from the differential absorption of left- and right-circularly polarized light by a chiral sample. The ECD scalar rotational strength of a given electronic transition, R_{n0}, is the dot product of the transition electric- and magnetic-dipole vectors, viz.

$$R_{n0} = \text{Im} \left\{ \langle \psi_0 | \boldsymbol{\mu} | \psi_n \rangle \cdot \langle \psi_n | \mathbf{m} | \psi_0 \rangle \right\}. \tag{25}$$

Thus, the theory underlying electronic circular dichroism spectra is closely related to that described earlier for optical rotation, and the determination of the rotational strength requires first the calculation of the excited-state wave functions and transition energies, followed by construction of either the individual transition moments or the analogous transition strengths.

Although much of the recent effort expended towards the ab initio computation of chiroptical properties has focused on optical rotation, ECD spectra can actually offer more infor-

mation regarding the relationship between the details of the molecular structure and its corresponding optical activity. ECD rotational strengths provide information about the structure in the vicinity of each absorbing chromophore in the molecule, as opposed to the single, composite property provided by optical rotation measurements. In this sense, ECD can sometimes offer a more valuable probe of absolute configuration than ORD. (However, it should be noted that many important chiral systems — including many natural products — do not lend themselves to convenient ECD analysis because they lack accessible chromophores.) Regardless, measurements of ECD spectra are performed less routinely by organic chemists than optical rotation, primarily because the experimental apparatus for the latter is much simpler to use and costs nearly an order of magnitude less to obtain. For overviews of the earliest computations of ECD spectra, including a discussion of the long-standing empirical and semi-empirical rules used to predict the signs of CD rotatory strengths, see the classic review by Hansen and Bouman [111] as well as the more recent contribution by Rauk [112].

3.1 Hartree-Fock and DFT ECD rotational strengths

Excited states are accessible within TD-HF/RPA [46, 44] or TD-DFT [47, 48] by diagonalization of the $\boldsymbol{\Gamma}$ matrix appearing in Eq. 6 with the metric Δ:

$$\boldsymbol{\Gamma Z} = \omega \Delta \boldsymbol{Z}, \tag{26}$$

where, again, the implied dimensions of the equation include all single excitations, $\boldsymbol{X}$, and de-excitations, $\boldsymbol{Y}$. In practice, the dimensions of the equation may be halved by inserting the definitions of $\boldsymbol{\Gamma}$, adding and substracting the resulting pair of matrix equations, and rearranging to obtain the non-Hermitian eigenvalue equation,

$$(\boldsymbol{A} - \boldsymbol{B})(\boldsymbol{A} + \boldsymbol{B})(\boldsymbol{X} + \boldsymbol{Y})_n = \omega_n^2 (\boldsymbol{X} + \boldsymbol{Y})_n, \tag{27}$$

where ω_n is the excitation energy and $\boldsymbol{X} + \boldsymbol{Y}$ is the corresponding eigenvector. Finally, the desired transition moments may be obtained as the dot product of this eigenvector with the electric- or magnetic-dipole integrals:

$$\langle \psi_0 | \mu_x | \psi_n \rangle = \boldsymbol{\mu}_x^+ (\boldsymbol{X} + \boldsymbol{Y})_n, \tag{28}$$

and

$$\langle \psi_n | m_x | \psi_0 \rangle = (\boldsymbol{X} + \boldsymbol{Y})_n^+ \boldsymbol{m}_x. \tag{29}$$

Equivalently, Eq. 27 may be subjected to a transformation to produce an Hermitian eigenvalue equation such that the left- and right-hand eigenvectors become simple adjoints of one another [44]. A related, but slightly simpler approach may be obtained using configuration interaction singles (CIS) [113] (also known as the Tamm-Dancoff approximation [114–117]), in which only the $\boldsymbol{A}$ submatrix from $\boldsymbol{\Gamma}$ in Eq. 26 is retained [118]:

$$\boldsymbol{A} \boldsymbol{X}_n = \omega_n \boldsymbol{X}_n. \tag{30}$$

Thus, the calculation of Hartree-Fock or DFT ECD rotational strengths requires the following additional steps beyond the initial calculation of the molecular orbitals:

1. Construction of the $\boldsymbol{A}$ and $\boldsymbol{B}$ matrices using the appropriate forms of Eqs. 9 and 10 (or just $\boldsymbol{A}$ for CIS-related methods).
2. Solution of the eigenvalue problem in Eq. 27 or Eq. 30 for each excited-state of interest.
3. Evaluation of the dot product in either Eq. 28 or 29 for each Cartesian component of the operator to obtain the required transition moment.

The final rotational strength is obtained as the dot product of the final transition moments, and thus requires little computational effort beyond the determination of the excited-state eigenvectors. ECD spectral simulations at the Hartree-Fock and DFT levels of theory have been implemented in several program packages [58, 59, 62, 68].

A major of advantage of TD-HF, CIS, and TD-DFT methods is their relative simplicity and computational efficiency. They are easily applied to excited states of molecules containing 20–30 non-hydrogen atoms. The primary disadvantage of TD-HF/RPA and CIS approaches is their lack of dynamic electron correlation effects, and, as a result, they often significantly overestimate excitation energies of closed-shell organic molecules [119]. TD-DFT methods offer substantial improvement over TD-HF and CIS and can often predict excitation energies to within 0.5 eV for well-localized states dominated by single-excitations. On the other hand, they are incapable of describing charge-transfer states without inclusion of exact Hartree-Fock exchange [120, 121], and they can dramatically underestimate excitation energies of diffuse, Rydberg states due to self-interaction errors [122]. Although one may compensate for the latter errors using various asymptotic corrections [123], such an approach may concomitantly produce inferior excited state properties and transition moments [124].

As for optical rotation, the spectre of origin-invariance again rears its ugly head in ECD rotational strength calculations, and, for incomplete basis sets, the above length-gauge representation of R_{n0} suffers from arbitrary origin dependence. Bak et al. [79] developed a GIAO-based implementations for both TD-HF/RPA theory and the related multiconfigurational RPA (MC-RPA) approach that avoid this problem in the same manner described earlier for optical rotation. More recently, Pecul et al. [125] reported the first GIAO-based DFT calculations of ECD spectra. Alternatively, as was described earlier for optical rotation, origin invariance of ECD rotational strengths may be achieved using a velocity-gauge representation for the electric-dipole operator, leading to the following expression for R_{n0},

$$R_{n0} = \frac{1}{\omega_{n0}} \text{Re} \left[\langle \psi_0 | \boldsymbol{p} | \psi_n \rangle \cdot \langle \psi_n | \mathbf{m} | \psi_0 \rangle \right]. \tag{31}$$

Most modern implementations of ECD spectra utilize the latter approach, which becomes equivalent to its length-gauge counterpart in the infinite-basis-set limit. However, as noted by Pecul et al. [125] the basis-set convergence of the velocity-gauge formulation appears to be slower than its length-gauge counterpart, even when GIAOs are not used in the latter.

Some of the earliest ab initio ECD calculations include those of Rauk, who applied truncated CI techniques to several small disulfides for comparison to previously reported semi-empirical calculations [126]. Shortly thereafter, Hansen and Bouman [127] applied an RPA-based (velocity-gauge) approach to *trans*-cyclooctene (TCO) (**20**) and 3-methylcyclopentene. They found that, although both molecules contain a central ethylene chromophore, qualitatively correct spectral assignments required simulation of the entire molecular structure rather than more convenient model systems. In the early 1990s, Peyerimhoff, Grimme, and co-workers reported a series of CI-based studies comparing theoretical and experimental rotational strengths for molecules such as substituted oxiranes, thiiranes, and cyclophanes [128–131]. Soon thereafter, the first density functional implementation of ECD rotational strengths was reported in 1996 by Grimme [132], who applied the DFT/CIS method (similar to that described above) in the length gauge to (*M*)-4,5-dimethylphenanthrene (**21**) and (*R*)-(+)-camphor (**10**) using the Turbomole package [59]. Later, Grimme and co-workers applied both the velocity-gauge TD-DFT approach and the length-gauge DFT/CIS approach to a series of large molecules,

including a number of cyclophane derivatives and helicenes, as well as camphor (**10**), norcamphor (**12**), and fenchone (**13**), and found reasonable agreement with experimental CD spectra [118,133]. Furche et al. [134] later reported large-scale DFT ECD calculations for a series of [*n*]-helicenes up to $n = 12$, as well as derivatives of hexahelicene. In 2002, Autschbach and co-workers developed an implementation of TD-DFT for ECD spectra within the ADF package [62,135], using both velocity- and length-gauge rotational strengths. They found that standard gradient corrected functionals produce the correct CD intensity difference, but, as is to be expected from TD-DFT, excitation energies tend to be underestimated, especially for Rydberg and charge-transfer states. Autschbach et al. [136] have also recently applied TD-DFT ECD simulations to cobalt and rhenium transition metal complexes, including solvent contiuum model corrections for the transition energies. [137] have very recently considered the influence of vibronic coupling on the ECD spectrum of dimethyloxirane (**7**), and solvent effects were included in recent DFT ECD spectral simulations by Pecul et al. [138] using the PCM.

Diedrich and Grimme [139] recently carried out a systematic comparison of the abilities of various ab initio methods for predicting ECD rotational strengths in a series of model systems, including H_2S_2 and twisted ethylene, and several "real-life" cases, such as camphor (**10**) and norcamphor (**12**). They considered a number of theoretical methods, including TD-DFT (with various functionals), as well as CC2 [101], multireference perturbation theory [140], and DFT/MRCI [141], using both length- and velocity-gauge expressions for the rotational strengths. They found systematically better performance for the DFT/MRCI and CC2 methods, though, among the standard functionals, B3LYP gave the best results.

In a particularly important *predictive* application [142], Stephens et al. [143] recently used DFT calculations of both optical rotation and electronic CD to assign the absolute configuration of a newly synthesized barrelenophane (**22**), whose enantiomers had been separated by chiral chromatography, but whose absolute configuration had not been previously assigned [142]. Using B3LYP/6-31G* structural optimizations of three important conformers, they generated Boltzmann averages of both $[\alpha]_{589}$ optical rotations and CD rotational strengths for comparison to the experimental data. Both optical rotation and CD agreed on the absolute configuration, perhaps lending greater confidence in the final assignment. We note, however, that the theoretical underpinnings of ECD and ORD are closely coupled (as indicated by the above discussion), and a given theoretical model may fail for both properties, thus limiting the predictive value of combined ECD/ORD simulations for assignments of absolute configuration in general.

3.2 ECD rotational strengths via coupled cluster theory

Coupled cluster theory offers a route to modeling electronic circular dichroism through its equation-of-motion (EOM-CC) [144] and linear response [64] variants in which excited states are approximated as eigenfunctions of the similarity-transformed Hamiltonian appearing in Eq. 13:

$$\mathrm{e}^{-\hat{T}}\hat{H}\mathrm{e}^{\hat{T}}\hat{R}_n|\psi_0\rangle = \bar{H}\hat{R}_n|\psi_0\rangle = E_n\hat{R}_n|\psi_0\rangle, \qquad (32)$$

where $\hat{R}_n$ is a cluster operator (analogous to $\hat{T}$) for the *n*-th excited state. Just as for the ground-state wave function, the non-Hermitian nature of the similarity-transformed Hamiltonian leads to a left-hand eigenvalue problem that is distinct from its right-hand counterpart, but with the same eigenvalues,

$$\langle\psi_0|\hat{L}_n\bar{H} = \langle\psi_0|\hat{L}_n E_n, \qquad (33)$$

where $\hat{L}_n$ is a de-excitation cluster operator and the excited-state counterpart of $\hat{R}_n$. The left- and right-hand excited state wave functions form a biorthogonal set,

$$\langle L_m|R_n\rangle \equiv \langle\psi_0|\hat{L}_m\hat{R}_n|\psi_0\rangle = \delta_{mn}. \qquad (34)$$

One method of defining the product of transition moments appearing in Eq. 25 is as the residue of the corresponding linear response function [45],

$$R_{n0} = \lim_{\omega\to\omega_{n0}}(\omega - \omega_{n0})\mathrm{Im}\langle\langle\boldsymbol{\mu};\mathbf{m}\rangle\rangle_\omega. \qquad (35)$$

Given coupled cluster left- and right-hand wave functions for the *n*-th excited state, the rotational strength may be computed as [64,145]

$$R_{n0} = \frac{1}{2}\left(\tilde{T}^n_{\boldsymbol{\mu}}\cdot T^n_{\mathbf{m}} + \left[\tilde{T}^n_{\mathbf{m}}\cdot T^n_{\boldsymbol{\mu}}\right]^*\right), \qquad (36)$$

where the right-hand wave function "transition moments" are defined as, for example,

$$\begin{aligned}\tilde{T}^n_{\boldsymbol{\mu}} &= \langle\psi_0|\hat{\Lambda}\left[\bar{\boldsymbol{\mu}},\hat{R}_n\right]|\psi_0\rangle \\ &+ \langle\psi_0|\hat{\Lambda}\left[\left[\bar{H},\hat{X}^\omega_\mu\right],\hat{R}_n\right]|\psi_0\rangle, \qquad (37)\end{aligned}$$

and their left-hand counterparts as,

$$T^n_\mu = \langle\psi_0|\left[\hat{L}_n,\bar{\boldsymbol{\mu}}\right]|\psi_0\rangle, \qquad (38)$$

where $\hat{\Lambda}$ is the same as that given for the left-hand ground-state wave function in Eq. 14. Thus, in this formulation, evaluation of the coupled cluster rotational strength of a given transition also requires the determination of a corresponding perturbed ground-state wave function, $\hat{X}^\omega_\mu$. Alternatively, one may choose to exclude the perturbed wave functions from Eq. 37, leading to a more efficient implementation. Although for small molecules this approximation makes little numerical difference, the resulting rotational strengths are not size-consistent [144].

Very few applications of coupled cluster theory to the determination of ECD rotational strengths have been reported thus far, and only the DALTON [68] and PSI3 [60] packages currently have this capability. Pedersen et al. [146] reported the first such calculations at the CCSD level in 1999. They explicitly considered both gauge and origin invariance in the scalar rotational strength and the rotational strength tensor, the latter of which provides CD intensity of oriented samples [147]. They applied this new technology to the twisted

ethylene chromophore of the popular TCO test case (**20**) and found that, contrary to conventional wisdom, the velocity-gauge expression for the rotational strength did not show slower basis-set convergence characteristics than its length-gauge counterpart. Pedersen and Koch [148] later extended this work to the ECD spectrum of the full molecule, and they suggested a slightly modified interpretation of the experimental spectrum.

4 Vibrational circular dichroism spectra

Like its ECD counterpart, vibrational circular dichroism (VCD) refers to the differential absorption intensities of left- and right-circularly polarized light by chiral molecules, but in this case, resulting in vibrational rather than electronic transitions. VCD provides even more information than either optical rotation or ECD regarding the relationship between molecular structure and optical activity owing to the fact that VCD rotational strengths may be measured even for molecules lacking a long-wavelength chromophore. However, experimental measurements of such spectra are carried out less often than their ORD and ECD counterparts due to the cost of the VCD apparatus and the high level of expertise required for its use.

Just as the oscillator strengths and integrated absorption intensities of simple vibrational absorption (infrared) spectra are related to the squares of electric-dipole transition moments [22],

$$D_{vv'}^n = \langle \Psi_{nv} | \hat{\boldsymbol{\mu}} | \Psi_{nv'} \rangle \cdot \langle \Psi_{nv'} | \hat{\boldsymbol{\mu}} | \Psi_{nv} \rangle, \tag{39}$$

the corresponding rotational strengths of VCD spectra are related to the dot product of the electric-dipole transition moment and the magnetic-dipole transition moment,

$$R_{vv'}^n = \mathrm{Im} \left\{ \langle \Psi_{nv} | \hat{\boldsymbol{\mu}} | \Psi_{nv'} \rangle \cdot \langle \Psi_{nv'} | \hat{\boldsymbol{m}} | \Psi_{nv} \rangle \right\}, \tag{40}$$

where n denotes the electronic state, v and v' denote vibrational states, and $|\Psi_{nv}\rangle$ and $|\Psi_{nv'}\rangle$ denote initial and final vibronic states, respectively.

We may compute the electric-dipole vibrational transition moment appearing in Eqs. 39 and 40 beginning from the Born-Oppenheimer approximation, in which we assume that the total vibronic wave function, $\Psi_{nv}(\boldsymbol{r}, \boldsymbol{R})$, may be written as a product of an electronic wave function, $\psi_n(\boldsymbol{r}; \boldsymbol{R})$ and a vibrational wave function, $\chi_{nv}(\boldsymbol{R})$, where $\boldsymbol{r}$ and $\boldsymbol{R}$ denote the collective electronic and nuclear coordinates, respectively. Then the electric-dipole transition matrix element may be written as

$$\langle \Psi_{nv}(\boldsymbol{r}, \boldsymbol{R}) | \hat{\boldsymbol{\mu}} | \Psi_{nv'}(\boldsymbol{r}, \boldsymbol{R}) \rangle$$
$$= \langle \chi_{nv}(\boldsymbol{R}) | \langle \psi_n(\boldsymbol{r}; \boldsymbol{R}) | \hat{\boldsymbol{\mu}} | \psi_n(\boldsymbol{r}; \boldsymbol{R}) \rangle | \chi_{nv'}(\boldsymbol{R}) \rangle$$
$$= \langle \chi_{nv} | \langle \hat{\boldsymbol{\mu}} \rangle_n | \chi_{nv'} \rangle \tag{41}$$

where $\langle \hat{\boldsymbol{\mu}} \rangle_n$ denotes the expectation value of the electric-dipole operator in the n-th Born-Oppenheimer electronic state. The dependence of the $\langle \hat{\boldsymbol{\mu}} \rangle_n$ on the nuclear coordinates is usually approximated by the first term of its Taylor expansion

about a reference geometry $\boldsymbol{R}^0$ (*i.e., the electrical harmonic approximation*):

$$\langle \hat{\boldsymbol{\mu}} \rangle_n \approx \langle \hat{\boldsymbol{\mu}} \rangle_0 + \sum_\alpha \left(\frac{\partial \langle \hat{\boldsymbol{\mu}} \rangle_n}{\partial R_\alpha} \right)_0 (R_\alpha - R_\alpha^0), \tag{42}$$

where the subscript 0 indicates that the given quantity is evaluated at the reference geometry. The dipole-moment derivatives may be easily computed using analytic gradient techniques, and the final expressions vary depending on the level of theory employed [149]. The total electric-dipole transition matrix element then becomes

$$\langle \Psi_{nv} | \hat{\boldsymbol{\mu}} | \Psi_{nv'} \rangle = \sum_\alpha \left(\frac{\partial \langle \hat{\boldsymbol{\mu}} \rangle_n}{\partial R_\alpha} \right)_0 \langle \chi_{nv} | (R_\alpha - R_\alpha^0) | \chi_{nv'} \rangle. \tag{43}$$

The vibrational wave functions, χ_{nv}, are usually taken to be harmonic oscillator functions (*i.e., the mechanical harmonic approximation*), which subsequently leads to relatively simple programmable equations in terms of the normal vibrational modes [150].

Unfortunately, the same approach fails for the magnetic-dipole vibrational transition moments appearing in Eq. 40 due to the fact that the electronic contribution to this transition moment vanishes:

$$\langle \psi_n(\boldsymbol{r}; \boldsymbol{R}) | \hat{\boldsymbol{m}}^{\mathrm{elec}} | \psi_n(\boldsymbol{r}; \boldsymbol{R}) \rangle$$
$$= -\frac{1}{2} \sum_i^{n_{\mathrm{elec}}} \langle \psi_n(\boldsymbol{r}; \boldsymbol{R}) | \boldsymbol{r}_i \times \boldsymbol{p}_i | \psi_n(\boldsymbol{r}; \boldsymbol{R}) \rangle = 0. \tag{44}$$

Because $\boldsymbol{m}$ is a time-odd operator, its expectation value must be zero for closed-shell (real) Born-Oppenheimer electronic wave functions [151].

In his pioneering paper on VCD in 1985 [152], Stephens showed how one can overcome this problem by introducing first-order non-adiabatic corrections to the Born-Oppenheimer wave function and subsequently evaluating these corrections as the leading terms of Taylor expansions of the adiabatic wave functions in the nuclear positions and an external magnetic field. This leads to an expression of the magnetic-dipole vibrational transition moment in terms of the overlap between wave function derivatives, viz. [152]

$$\langle \Psi_{nv} | (\hat{\boldsymbol{m}}^{\mathrm{elec}})_\beta | \Psi_{nv'} \rangle$$
$$= -2\hbar \omega_{vv'} \sum_\alpha \left\langle \left(\frac{\partial \psi_n}{\partial R_\alpha} \right)_0 \middle| \left(\frac{\partial \psi_n}{\partial B_\beta} \right)_0 \right\rangle \times$$
$$\langle \chi_{nv} | (R_\alpha - R_\alpha^0) | \chi_{nv'} \rangle, \tag{45}$$

where ω is the angular frequency of the vibrational transition, B_β denotes a particular Cartesian component of a "false" external magnetic field, and we have suppressed the explicit dependence of the wave functions on $\boldsymbol{r}$ and $\boldsymbol{R}$ for notational simplicity. Again, the matrix element of the displacement coordinate, $R_\alpha - R_\alpha^0$ is easily evaluated assuming harmonic oscillator functions, as for the electric-dipole transition moment. Thus, the electronic contribution to the elusive magnetic-dipole vibrational transition moment requires computation of the derivatives of the wave function with respect

to the nuclear coordinates — a derivative that is also implicitly required for the corresponding electric-dipole transition moment — and with respect to an external magnetic field.

An alternative perspective was offered by Buckingham et al. [153, 154] who preferred to consider a Taylor expansion of the electronic contributions to the time-odd magnetic-dipole operator in odd powers of the nuclear *velocities*, e.g.

$$\boldsymbol{m} = \sum_\alpha \left(\frac{\partial \boldsymbol{m}}{\partial \dot{R}_\alpha}\right)_0 (\dot{R}_\alpha - \dot{R}_\alpha^0)$$
$$+ \sum_{\alpha\beta} \left(\frac{\partial^2 \boldsymbol{m}}{\partial \dot{R}_\alpha \partial R_\beta}\right) (\dot{R}_\alpha - \dot{R}_\alpha^0)(R_\beta - R_\beta^0) + \cdots ,$$

(46)

where the dot indicates derivative with respect to time. This leads to an expression for the vibrational transition moment,

$$\langle \Psi_{nv}|(\hat{m}^{\text{elec}})_\beta|\Psi_{nv'}\rangle$$
$$= \langle \chi_{nv}|\dot{\boldsymbol{R}}|\chi_{nv'}\rangle \cdot \frac{\partial(\hat{m}^{\text{elec}})_\beta}{\partial \dot{\boldsymbol{R}}}$$
$$= 2\hbar \langle \chi_{nv}|\dot{\boldsymbol{R}}|\chi_{nv'}\rangle \cdot \text{Im}\left\langle \left(\frac{\partial \psi_n}{\partial \boldsymbol{R}}\right)_0 \middle| \left(\frac{\partial \psi_n}{\partial B_\beta}\right)_0 \right\rangle ,$$

(47)

that is equivalent to Eq. 45. The advantage of this approach is primarily conceptual: the expansion of the magnetic-dipole operator in terms of nuclear velocities allows a relatively simple physical interpretation of VCD rotational strengths in terms of induced, infinitesimal electronic currents near the nuclei.

The Born-Oppenheimer separation of electronic and vibrational wave functions allows for the evaluation of VCD rotational strengths via separate calculations of the vibrational transition moments appearing in Eq. 40. Thus, to enforce origin invariance of the total VCD rotational strength, one must ensure that the individual vibrational transition moments are themselves origin independent. While the electric-dipole transition moment is trivially origin invariant for the length-gauge representation, this is not the case for the magnetic-dipole transition moment. We note in passing that a simple velocity-gauge transformation without extension beyond the Born-Oppenheimer approximation of the electric-dipole operator would, in fact, lead to a vanishing rotational strength because, like the magnetic-dipole operator, the linear momentum operator is time-odd, *ergo*,

$$\langle \psi_n(\boldsymbol{r}; \boldsymbol{R})|\hat{\boldsymbol{p}}|\psi_n(\boldsymbol{r}; \boldsymbol{R})\rangle = 0.$$

(48)

Thus, in order for ab initio computations of VCD spectra to achieve origin invariance, one must adopt a formulation that enforces this property directly for the magnetic-dipole operator itself, perhaps through the use of GIAOs [75] or other methods (*vide infra*) [155].

4.1 Ab initio implementation of VCD spectra

The tremendous advances in analytic derivative methods over the last several decades have made possible the ab initio calculation of VCD rotational strengths. At the Hartree-Fock

and DFT levels, for example, the overlap of wave function derivatives appearing in Eq. 45 simplifies to

$$\left\langle \left(\frac{\partial \psi_n}{\partial R_\alpha}\right)_0 \middle| \left(\frac{\partial \psi_n}{\partial B_\beta}\right)_0 \right\rangle = \sum_i^{\text{occ}} \left\langle \left(\frac{\partial \phi_i}{\partial R_\alpha}\right)_0 \middle| \left(\frac{\partial \phi_i}{\partial B_\beta}\right)_0 \right\rangle , \quad (49)$$

where ϕ_i denotes the i-th occupied Hartree-Fock or Kohn-Sham molecular orbital. The derivatives of the molecular orbitals are routinely computed by means of the corresponding coupled-perturbed Hartree-Fock (CPHF) or Kohn-Sham (CPKS) equations. The precise form of these equations depends on the nature of the perturbation and may be obtained by differentiation of the appropriate variational (Brillouin) condition with respect to the perturbation:

$$(\boldsymbol{A} \pm \boldsymbol{B})\boldsymbol{U}^x = \boldsymbol{Z}^x,$$

(50)

where the matrices $\boldsymbol{A}$ and $\boldsymbol{B}$ are the same as those defined earlier in Eqs. 9 and 10. The positive combination, $\boldsymbol{A} + \boldsymbol{B}$, is known as the "electric Hessian" and is obtained for real perturbations, such as nuclear coordinates or external electric fields, while $\boldsymbol{A} - \boldsymbol{B}$ (the "magnetic Hessian") results for pure imaginary perturbations [156]. The components of the $\boldsymbol{U}$ vector represent the derivatives of the molecular orbital coefficients, which are expanded as linear combinations of the unperturbed coefficients, e.g. [149],

$$\frac{\partial C_\nu^i}{\partial x} = \sum_p U_{pi}^x C_\nu^p.$$

(51)

The form of the perturbation-dependent term, $\boldsymbol{Z}^x$, varies depending on the nature of the perturbation as well as whether the atomic orbital (AO) basis functions depend explicitly on the perturbation. For electric or magnetic fields without field-dependent AO's, $\boldsymbol{Z}^x$ simplifies to electric or magnetic dipole integrals, for example.

Hartree-Fock and DFT calculations of VCD rotational strengths therefore require several steps:

1. Evaluation of the harmonic force field and corresponding normal coordinates for the given optimized geometry. This step implicitly requires the solutions of the CPHF/CPKS equations for nuclear perturbations, R_α.
2. Evaluation of the derivatives of the electric-dipole moment, followed by their transformation into the normal coordinate basis for the construction of the electric-dipole transition moments in Eq. 43. (These quantities are also required for conventional infrared absorption spectra, as is apparent from Eq. 39.)
3. Solution of the CPHF/CPKS equations for magnetic field perturbations, B_β, to obtain the MO derivatives, $\partial \phi_i / \partial B_\beta$.
4. Construction of the magnetic-dipole transition moments in Eq. 45 as overlaps of the MO derivatives, followed by their transformation into the normal coordinate basis.

The final rotational strengths in Eq. 40 are then computed as simple dot products of the electric- and magnetic-dipole transition moments. The most computationally intensive step is the evaluation of the harmonic force field itself due to the need to compute analytic first- and second-derivative integrals for

each perturbation, as well as the solution of the CPHF/CPKS equations for nuclear perturbations. Thus, the additional steps required for simulation of VCD spectra within Hartree-Fock theory or DFT are relatively inexpensive.

For coupled cluster methods, the overlap expression appearing in Eq. 45 must be evaluated with appropriate consideration of the differing left- and right-hand coupled cluster wave functions in Eqs. 12 and 14. Although no coupled cluster implementations of VCD spectra have yet been reported in the literature, the foundations for such calculations have already been laid. Derivatives of $\hat{T}$ and $\hat{\Lambda}$ with respect to nuclear coordinates are required to evaluate the harmonic force field [157–159], and analogous derivatives with respect to an external magnetic field are required for NMR chemical shielding tensors [160]. For methods such as CCSD, these derivatives (along with associated orbital relaxation terms) may be used directly to evaluate Eq. 45, while for methods without well-defined wave functions, such as CC2 [101], CCSD(T) [161, 162], CCSDT-n [163], CC3 [72], etc., response or equation-of-motion approaches may be necessary.

4.2 Applications

The first implementation of VCD rotational strengths using ab initio methods was reported in 1986 at the Hartree-Fock level by Lowe et al. [164, 165] who evaluated the molecular orbital derivatives in Eq. 49 using numerical differentiation techniques. Soon thereafter, Amos, Handy, Jalkanen, and Stephens implemented the more efficient analytic derivative approach described above within the CADPAC program suite [57] and applied it to isotopomers of ethylene oxide (oxirane) [166]. Morokuma and Sugeta [167] reported an independent implementation using analytic derivatives for the nuclear perturbations and numerical differentiation for the magnetic-field perturbations shortly thereafter. Amos et al. [168] reported the first VCD calculations including electron correlation effects in 1990 using second-order perturbation theory (MP2) for the harmonic force field and electric-dipole derivative contributions, but retaining the SCF-level description of the magnetic-dipole transition moment. In their test calculations on (*R*)-methylthiirane, they reported that electron correlation effects were vital to obtain the correct signs for the rotational strengths in all regions of the spectrum. Stephens et al. [169, 170] used the same approach for *trans*-2,3-dideuteriooxirane, methyloxirane (**6**), and deutero-cyclopropanes with somewhat larger basis sets and found that the VCD rotational strengths compared well with experiment for almost all transitions, apart from Fermi resonances in the C−H stretching regions. They noted that "errors in rotational strengths arising from the absence of electron correlation...are not insignificant [169]."

Although origin invariance was not achieved for many of the early calculations of ab initio VCD spectra, Stephens suggested the use of a "distributed origin" (DO) approach whereby each atomic contribution to the total magnetic-dipole transition moment [referred to as the atomic axial tensor (AAT)] is assigned its own origin, namely the position of the given nucleus [155]. The resulting expressions allow for the computation of the AATs in terms of their electric-dipole counterparts [known as atomic polar tensors (APTs)], written in the velocity-gauge [171]. This approach guarantees overall origin independence of the computed rotation strengths, and was used in a number of applications, including those by Stephens et al. [169, 170] described above. (The DO approach was also utilized by Yang and Rauk [172] within the vibrational coupling theory of Nafie) Bak et al. [173, 174] have criticised this approach, however, on the grounds that the basis-set convergence behavior of the AATs with DOs is somewhat slower than for the APTs. To overcome this problem while still maintaining origin invariance, Bak et al. reported the first use of GIAOs for VCD calculations at the SCF and MCSCF levels of theory in 1993, and reported tests of the method's basis-set convergence properties soon thereafter.

In 1994, Stephens et al. [175] reported the first simulations of VCD spectra using DFT. They computed the harmonic force field and APTs using a variety of density functionals (LDA, BLYP, B3LYP), and approximated the AATs using the DFT-based APTs coupled to SCF-level AATs in the common origin. Based on a series of test calculations for 4-methyl-2-oxetanone (**23**), 6,8-dioxabicyclo[3.2.1]octane (**24**), and camphor (**10**), they concluded that B3LYP provides comparable accuracy to the MP2 methods mentioned above, but with considerably improved disk-storage requirements.

The current state-of-the-art in ab initio VCD rotational strength calculations was reported by Cheeseman et al. [176] in 1996 with the development of the first GIAO-based DFT codes. In an analysis of their detailed calculations on *trans*-2,3-dideuteriooxirane, they attributed the remaining few discrepancies between theory and experiment to deficiencies in the latter. Since this new approach was first made available in the Gaussian programs [58], the vast majority of VCD calculations reported in the literature have made use of GIAO-DFT methodology. Excellent overviews of a number of important applications have been recently given by Stephens and Devlin [30] and by Freedman et al. [31] Apart from the need to consider higher levels of electron correlation in the electronic structure model, most of the remaining discrepancies between theory and experiment can likely be attributed to anharmonicity [177] (especially in higher-frequency C−H stretching regions) and solvent effects. (Recent work by Cappelli et al. [178] on PCM-based VCD simulations of 3-butyn-2-ol have highlighted the latter). In addition, recent work by Polavarapu et al. [179, 180] has indicated the need for improved quantitative accuracy in VCD rotational strengths for the determination of conformer populations.

5 Raman optical activity

The phenomenon of Raman optical activity (ROA) arises due to the weak differential scattering of left- and right-circularly polarized light by chiral molecules. Although initially

hampered by instrumentation obstacles, ROA has blossomed in recent years as a potentially potent technique for structure determination in a wide variety of chiral molecules, ranging from small systems such as methyloxirane, to biological species as large as viruses [181, 182]. Barron et al. [33] have recently offered a concise and readable review of the history and theoretical foundations of ROA, as well as a number of its most recent applications.

The first complete theoretical description of ROA was given in 1971 by Barron and Buckingham [183], who introduced the unitless circular intensity difference (CID),

$$\Delta = (I^R - I^L)/(I^R + I^L), \tag{52}$$

where I^R and I^L are the individual scattering intensities [184]. The first confirmed experimental observation of ROA was reported Barron et al. [185] 2 years later. Barron and Buckingham demonstrated that the numerator and denominator in the above expression may be related to molecular parameters by consideration of the field vectors radiated by oscillating electric-dipole, magnetic-dipole, and electric-quadrupole moments, leading to expressions for the Rayleigh optical scattering CIDs of a number of relevant experimental scattering geometries, such as depolarized scattering,

$$\Delta_z(90^o) = \frac{12[\beta(G')^2 - (1/3)\beta(A)^2]}{6c\beta(\alpha)^2}, \tag{53}$$

and in-phase dual circular polarization (DCP) backscattering,

$$\Delta^{DCP_I}(180^o) = \frac{48[\beta(G')^2 + (1/3)\beta(A)^2]}{12c\beta(\alpha)^2}. \tag{54}$$

These equations require orientationally averaged expressions for the isotropic and anisotropic tensor-component products of the electric-dipole polarizability, $\alpha_{\alpha\beta}$ (Eq. 4), the electric-dipole/magnetic-dipole polarizability, $G'_{\alpha\beta}$ (which is identical to the Rosenfeld β tensor of Eq. 3), and the electric-dipole/electric-quadrupole polarizability, $A_{\alpha\beta\gamma}$, viz.,

$$\beta(\alpha)^2 = \frac{1}{2}\left(3\alpha_{\alpha\beta}\alpha_{\alpha\beta} - \alpha_{\alpha\alpha}\alpha_{\beta\beta}\right), \tag{55}$$

$$\beta(G')^2 = \frac{1}{2}\left(3\alpha_{\alpha\beta}G'_{\alpha\beta} - \alpha_{\alpha\alpha}G'_{\beta\beta}\right), \tag{56}$$

and

$$\beta(A)^2 = \frac{1}{2}\omega_0\alpha_{\alpha\beta}\epsilon_{\alpha\gamma\delta}A_{\gamma\delta\beta}. \tag{57}$$

The subscript Greek letters in these equations refer to cartesian components, $\epsilon_{\alpha\gamma\delta}$ is the third-order Levi-Civita tensor, ω_0 is the incident laser frequency, and the Einstein summation convention is implied.

In vibrational Raman scattering, the electronic polarizability tensors above must be replaced by the corresponding vibrational transition moments, e.g., $\langle\chi_{nv}|\alpha_{\alpha\beta}(R_\gamma - R_\gamma^0)|\chi_{nv'}\rangle$. The necessary polarizabilities may then be expanded in Taylor series about the equilibrium geometry, and the Placzek approximation assumes that only the linear contribution in this expansion contributes significantly [186]. This leads to final expressions for the above tensor products in terms of

derivatives of the polarizabilities with respect to normal coordinates, $Q_{vv'}$, e.g. [80,22],

$$\langle\chi_{nv}|\alpha_{\alpha\beta}|\chi_{nv'}\rangle\langle\chi_{nv'}|\alpha_{\alpha\beta}|\chi_{nv}\rangle$$
$$\approx \frac{1}{2\omega_{vv'}}\left(\frac{\partial\alpha_{\alpha\beta}}{\partial Q_{vv'}}\right)_0\left(\frac{\partial\alpha_{\alpha\beta}}{\partial Q_{vv'}}\right)_0. \tag{58}$$

Thus, ab initio computation of ROA CIDs requires differentiation of the polarizability tensors, α, G', and A, with respect to the nuclear coordinates. Although analytic derivative methods exist for the electric dipole polarizability [187, 188], no such procedures have yet been reported for derivatives of the G' tensor, and thus nearly all ROA calculations reported in the literature make use of numerical differentiation techniques. (See the text by Polavarapu [29] for a detailed assessment of the fundamental equations of ROA.)

Origin dependence of ROA CIDs arises both from the appearance of the magnetic-dipole operator in the definition of the G' tensor (see Eq. 3) and from the definition of the electric quadrupole tensor, A [22]. However, unlike optical rotation and ECD rotational strengths, a velocity-gauge representation of the electric-dipole operator cannot circumvent this problem because of the appearance of off-diagonal components of G' in Eq. 56. [Note that for optical rotation and ECD, only the trace of G' is needed, as illustrated in Eq. 20.] Thus, the only option is to adopt a method for which origin invariance is independently enforced such that the origin dependence of each component of G' correctly cancels that of the components of the A tensor. This can be accomplished using GIAOs for Hartree-Fock and DFT, whose response functions then satisfy Eq. 21, but not for coupled cluster methods, even in the limit of a complete basis set [66,81].

5.1 Ab initio calculation of Raman optical activity

Ab initio ROA calculations have been implemented in a number of publicly available packages at the Hartree-Fock and DFT levels of theory [61,58,59]. The first such calculations of ROA CIDs were reported in 1989 and 1990 by Polavarapu et al. [189–191] using Hartree-Fock theory and small basis sets (6-31G, 6-31G*, and 6-31G**) for a number of small molecules, including H_2O_2, D_2O_2, methyloxirane (**6**), and methylthiirane. The necessary polarizability derivatives (using the static-field limit formulation by Amos [54]) were evaluated numerically by finite displacements of the molecular geometry around equilibrium, with the coordinate origin chosen arbitrarily either at the center of charge or mass, a small distance away along a coordinate axis, or at an atom. Later, these same researchers extended this work by making use of MP2-level harmonic force fields, combined with Hartree-Fock-level calculations of the polarizabilities derivatives (again evaluated by finite difference techniques) [192].

The first origin-independent and frequency-dependent ROA CID calculations were reported in 1994 by Helgaker et al. [80] using GIAOs at the Hartree-Fock level of theory. Using methyloxirane (**6**) as a test case, they found significant discrepancies between theory and experiment and concluded

that electron correlation effects and anharmonicity corrections would be necessary to resolve them. They also noted that, similarly to other chiroptical properties such as optical rotation, large basis sets including diffuse functions are required to obtain converged results. This latter point was emphasized recently by Pecul and Rizzo [193] who noted that the aug-cc-pVXZ and d-aug-cc-pVXZ basis sets of Dunning et al. [194–196] yielded significantly improved results. Zuber and Hug [197] recently reported that diffuse higher-angular-momentum functions for the hydrogen atoms are vital for qualitatively correct ROA CIDs, and that the aug-cc-pVXZ basis sets of Dunning et al. [198, 199] yielded significant improvements over Pople-type split valence basis sets. (This point is similar to that made by Wiberg et al. [97] in a careful study of basis-set effects on optical rotation in ethane in 2004, as discussed earlier.) In addition, they developed a small basis set without polarization functions that performs essentially as well as the aug-cc-pVDZ basis set for considerably less computational cost.

Bouř has recently introduced an alternative approach to ROA spectra that avoids the linear response approach to the polarizability tensors in favor of a truncated summation of, for example, Eq. 3, known as the sum-over-states (SOS) approach [200, 201]. For the special cases of Hartree-Fock and DFT theory, Bouř demonstrated that the final equations could be approximated well using only singly excited determinants for the excited states (which also leads to simplified excitation energies), and that analytic expressions for the polarizability derivatives with respect to nuclear coordinates were straightforward. In addition, he enforced origin independence of the G' tensor through a distributed origin approach, comparable to that used by Stephens [155] in the evaluation of VCD rotational strengths. Test calculations on α-pinene (**14**) and model peptides demonstrated that the SOS approach provides reasonable accuracy, but at substantially reduced computational cost relative to linear-response schemes.

Ruud et al. [202] recently reported the first DFT-level implementation of ROA CIDs using GIAOs, and numerical differentiation of the relevant frequency-dependent polarizabilites. Their work indicated that, in spite of earlier suggestions that correlation effects might be significant, differences between Hartree-Fock and DFT ROA CIDs are relatively small, though for accurate quantitative calculations of the detailed ROA spectrum, DFT represents the current state of the art. In addition, they compared their results to those from Bouř's [200, 201] approach above, and concluded that the SOS method is a "fast and inexpensive tool for quickly providing theoretical CIDs that may help in the first assignment of the experimental VROA spectra."

Just as for other chiroptical properties, solvent and/or conformational effects can be significant for ROA CIDs. Several recent studies have addressed one or both of these problems for a number of biologically relevant examples, including small dipeptides and carbohydrates [197, 203–206]. For example, Bouř et al. recently examined the ROA spectra of the L-alanyl-L-alanine zwitterionic dipeptide for which a number of low-lying conformers exist whose relative ener-

gies depend greatly on the use of solvent corrections (e.g., the Onsager model). Using DFT harmonic force fields coupled with Hartree-Fock-level polarizability derivatives, they reported ROA spectra that allowed assignment of most of the experimentally observed vibrational bands [203].

One of the difficulties of ab initio evaluation of ROA CIDs (as for many other properties) is analyzing the computed results in terms of individual wave function or atomic contributions. Although first-principles models are often capable of producing very accurate results, they also can provide far too much data to allow for deeper insight into the most important contributions to the CID of a particular vibrational mode. In an effort to overcome this problem, Hug [207] recently introduced a scheme for visualizing ROA contributions to vibrational modes via an atomic decomposition [the Raman atomic contribution pattern (ACP)] of the polarizability derivatives. These techniques were subsequently applied to an ROA CID analysis of the σ-helicene [4]triangulane (**18**) [208] and, more recently, to the assignment of the absolute configurations of individual stereogenic centers in *Galaxolide©* (1,3,4,6,7,8- hexahydro-4,6,6,7,8,8-hexamethylindeno [5,6-*c*]pyran, **25**) [209].

6 Summary and prospectus

Thanks in part to advances in response theories and analytic derivative techniques, the last several years have witnessed tremendous progress in ab initio methods for computing chiroptical properties, including optical rotation, ECD, VCD, and ROA. State-of-the-art implementations of TD-DFT and coupled cluster approaches for optical rotation, in particular, have been applied to chiral molecules containing thirty atoms or more. DFT treatments of VCD rotational strengths have been invaluable for a number of definitive assignments of absolute configuration, and the emerging techniques for modeling ROA spectra will likely prove to be at least equally valuable.

Much work remains to be done, however, before ab initio models can provide the accuracy and reliability needed for deeper insight into chiroptical response. It is not yet known, for example, what level of rigor is required in terms of basis set completeness or the treatment of dynamic electron correlation to reproduce even gas-phase optical rotation measurements reliably to within $10 \deg \mathrm{dm}^{-1} (\mathrm{g/mL})^{-1}$ (a level of accuracy that may well be essential for the assignment of absolute configuration for complicated structures). Zero-point vibrational effects are rarely considered, but may be necessary even to obtain the correct sign of optical rotation or ECD rotational strengths for some systems [110]. For conformationally flexible molecules, a common approach is to use a Boltzmann averaging procedure of the property of interest for a few relevant minima, but for many molecules, the energetic barriers separating these minima are likely to be too small to discount vibrational tunnelling effects. Finally, solvent perturbations on chiroptical properties are known to be large in many cases, and although PCM calculations have offered improved agreement between theory and experiment,

explicit solvation modeling may eventually be needed to account for the numerous remaining discrepancies.

Nevertheless, as we continue to learn about the fundamental nature of optical activity through the interplay of theoretical modeling and new experimental technology, there is good reason to remain optimistic that the promise of a suite of computational tools for assisting in the determination of the absolute configurations of chiral molecules will soon become a reality.

7 Acknowledgments

References

1. Eliel EL, Wilen SH (1994) Stereochemistry of organic compounds. Wiley, New York
2. Friedman L, Miller JG (1971) Science 172:1044
3. Wnendt S, Zwingenberger K (1997) Nature 385:303
4. Lee TJ, Scuseria GE (1995) In: Langhoff SR (eds) Quantum mechanical electronic structure calculations with chemical accuracy. Kluwer, Dordrecht, pp 47–108
5. Helgaker T, Jørgensen P, Olsen J (2000) Molecular electronic structure theory. Wiley, New York
6. Helgaker T, Ruden TA, Jørgensen P, Olsen J, Klopper W (2004) J Phys Org Chem 17:913
7. Snatzke G (1979) Angew Chem Int Ed Engl 18:363
8. Rinderspacher BC, Schreiner PR (2004) J Phys Chem A 108:2867
9. Goddard WA (1985) Science 227:917
10. Parr RG, Yang W (1989) Density-functional theory of atoms and molecules. Oxford University, New York
11. Bartlett RJ (1995) In: Yarkony DR (eds) Modern electronic structure theory, vol 2 of Advanced series in physical chemistry. World Scientific, Singapore, Chap16, pp. 1047–1131
12. Crawford TD, Schaefer HF (2000) In: Lipkowitz KB, Boyd DB (eds) Reviews in Computational Chemistry, vol 14, Chap. 2. VCH Publishers, New York, pp 33–136
13. Møller C, Plesset MS (1934) Phys Rev 46:618
14. Bartlett RJ (1981) Annu Rev Phys Chem 32:359
15. Becke AD (1993) J Chem Phys 98:5648
16. Lee C, Yang, Parr RG (1988) Phys Rev B 37:785
17. Pulay P (1983) Chem Phys Lett 100:151
18. Sæbø S, Pulay P (1993) Ann Rev Phys Chem 44:213
19. Hampel C, Werner H-J (1996) J Chem Phys 104:6286
20. Schütz M (2002) Phys Chem Chem Phys 4:3941
21. Russ NJ, Crawford TD (2004) Chem Phys Lett 400:104
22. Barron LD (2004) Molecular Light scattering and optical activity, 2nd edn. Cambridge University Press, Camridge
23. Caldwell DJ, Eyring H (1971) The theory of optical activity. Wiley, New York
24. Charney E (1979) The molecular basis of optical activity: optical rotatory dispersion and circular dichroism. Wiley, New York
25. Mason SF (1982) Molecular optical activity and the chiral discriminations. Cambridge University Press, Cambridge
26. Polavarapu PL (2002) Chirality 14:768
27. Stephens RJ, Devlin FJ, Cheeseman JR, Drisch MJ, Bortolini O, Besse P (2003) Chirality 15:S57
28. Stephens PJ, McCann DM, Cheeseman JR, Frisch MJ (2005) Chirality 17:S52
29. Polavarapu PL (1998) Vibrational spectra: principles and applications with emphasis on optical activity, vol 85 of studies in physical and theoretical chemistry. Elsevier, Amsterdam
30. Stephens PJ, Devlin FJ (2000) Chirality 12:172
31. Freedman TB, Cao X, Dukor RK, Nafie (2003) Chirality 15:743
32. Nafie LA (1997) Ann Rev Phys Chem 48:357
33. Barron LD, Hecht L, McColl IH, Blanch EW (2004) Mol Phys 102:731
34. Wagnière GH (1999) Chem Phys 245:165
35. Coriani S, Jørgensen P, Rizzo A, Ruud K, Olsen J (1999) Chem Phys Lett 300:61
36. Coriani S, Pecul M, Rizzo A, Jørgensen P, Jaszunski M (2002) J Chem Phys 117:6417
37. Rizzo A, Kallay M, Gauss J, Pawlowski F, Jørgensen P, Hättig C (2004) J Chem Phys 121:9461
38. Ekstrom U, Norman P, Rizzo A (2005) J Chem Phys 122:074321
39. Kirkwood J, Albrecht AC, Fischer P, Buckingham AD (2002) In: Hicks J (ed) Chirality: physical chemistry, vol 810 of ACS symposium series Chap. 10. Oxford University Press, Oxford, pp 130–144
40. Stephens PJ (1970) J Chem Phys 52:3489
41. Stephens PJ (1976) Adv Chem Phys 35:197
42. Buckingham AD (2004) Chem Phys Lett 398:1
43. Rosenfeld L (1928) Z Physik 52:161
44. Jørgensen P, Simons J (1981) Second quantization-based methods in quantum chemistry. Academic, New York
45. Linderberg J, Öhrn Y (2004) Propagators in quantum chemistry, 2nd edn. Wiley, New Jersey
46. Rowe DJ (1968) Rev Mod Phys 40:153
47. Casida ME (1995) In: Chong DP (ed) Recent advances in density functional methods, vol 1. World Scientific, Singapore
48. Bauernschmitt R, Ahlrichs R (1996) Chem Phys Lett 256:454
49. Grimme S (2001) Chem Phys Lett 339:380
50. Ruud K, Helgaker T (2002) Chem Phys Lett 352:533
51. Furche F (2001) J Chem Phys 114:5982
52. Autschbach J, Patchkovskii S, Ziegler T, van Gisbergen S, Baerends EJ (2002) J Chem Phys 117:581
53. Polavarapu PL (1997) Mol Phys 91:551
54. Amos RD (1982) Chem Phys Lett 87:23
55. Cheeseman JR, Frisch MJ, Devlin FJ, Stephens PJ (2000) J Phys Chem A 104:1039
56. Stephens PJ, Devlin FJ, Cheeseman JR, Frisch MJ (2001) J Phys Chem A 105:5356
57. Amos RD, Alberts IL, Andrews JS, Colwell SM, Handy NC, Jayatilaka D, Knowles PJ, Kobayashi R, Laidig KE, Laming G, Lee AM, Maslen PE, Murray CW, Rice JE, Simandiras ED, Stone AJ, Su M-D, Tozer DJ (1995) CADPAC: The Cambridge Analytic Derivatives Package Issue 6, Cambridge. A suite of quantum chemistry programs
58. Frisch MJ, Trucks GW, Schlegel HB, Scuseria GE, Robb MA, Cheeseman JR, Montgomery JA Jr, Vreven T, Kudin KN, Burant JC, Millam JM, Iyengar SS, Tomasi J, Barone V, Mennucci B, Cossi M, Scalmani G, Rega N, Petersson GA, Nakatsuji H, Hada M, Ehara M, Toyota K, Fukuda R, Hasegawa J, Ishida M, Nakajima T, Honda Y, Kitao O, Nakai H, Klene M, Li X, Knox JE, Hratchian HP, Cross JB, Adamo C, Jaramillo J, Gomperts R, Stratmann RE, Yazyev O, Austin AJ, Cammi R, Pomelli C, Ochterski JW, Ayala PY, Morokuma K, Voth GA, Salvador P, Dannenberg JJ, Zakrzewski VG, Dapprich S, Daniels AD, Strain MC, Farkas O, Malick DK, Rabuck AD, Raghavachari K, Foresman JB, Ortiz JV, Cui Q, Baboul AG, Clifford S, Cioslowski J, Stefanov BB, Liu G, Liashenko A, Piskorz P, Komaromi I, Martin RL, Fox DJ, Keith T, Al-Laham MA, Peng CY, Nanayakkara A, Challacombe M, Gill PMW, Johnson B, Chen W, Wong MW, Gonzalez C, Pople JA (2003) GAUSSIAN-03. Gaussian, Inc., Pittsburg

59. Ahlrichs R, Bärand M, Baron H-P, Bauernschmitt R, Böcker S, Deglmann P, Ehrig M, Eichkorn K, Elliott S, Furche F, Haase F, Häser M, Horn H, Hättig C, Huber C, Huniar U, Kattannek M, Köhn A, Kölmel C, Kollwitz M, May K, Ochsenfeld C, Ohm H, Patzelt H, Rubner O, Schäfer A, Schneider U, Sierka M, Treutler O, Unterreiner B, von Arnim M, Weigend F, Weis P, Weiss H (2002) Turbomole v5.6

60. Crawford TD, Sherrill CD, Valeev EF, Fermann JT, King RA, Leininger ML, Brown ST, Janssen CL, Seidl ET, Kenny JP, Allen WD (2003) PSI 3.2

61. DALTON, a molecular electronic structure program, Release 2.0 (2005) see http://www.kjemi.uio.no/software/dalton/dalton.html

62. Amsterdam Density Functional program, Theoretical Chemistry, Vrije Universiteit, Amsterdam, http://www.scm.com

63. Grimme S, Furche F, Ahlrichs R (2002) Chem Phys Lett 361:321

64. Koch H, Jørgensen P (1990) J Chem Phys 93:3333

65. Christiansen O, Jørgensen P, Hättig C (1998) Int J Quantum Chem 68:1

66. Pedersen TB, Koch K (1997) J Chem Phys 106:8059

67. Ruud K, Stephens PJ, Devlin FJ, Taylor PR, Cheeseman JR, Frisch MJ (2003) Chem Phys Lett 373:606

68. Helgaker T, Jensen HJAa, Jørgensen P, Olsen J, Ruud K, Ågren H, Auer AA, Bak KL, Bakken V, Christiansen O, Coriani S, Dahle P, Dalskov EK, Enevoldsen T, Fernandez B, Hättig C, Hald K, Halkier A, Heiberg H, Hettema H, Jonsson D, Kirpekar S, Kobayashi R, Koch H, Mikkelsen KV, Norman P, Packer MJ, Pedersen TB, Ruden TA, Sanchez A, Saue T, Sauer SPA, Schimmelpfennig B, Sylvester-Hvid KO, Taylor PR, Vahtras O (2005) Dalton, a molecular electronic structure program, Release 2.0

69. Tam MC, Russ NJ, Crawford TD (2004) J Chem Phys 121:3550

70. Crawford TD, Owens LS, Tam MC, Schreiner PR, Koch H (2005) J Am Chem Soc 127:1368

71. Kongsted J, Pedersen TB, Strange M, Osted A, Hansen AE, Mikkelsen KV, Pawlowski F, Jørgensen P, Hättig C (2005) Chem Phys Lett 401:385

72. Koch H, Christiansen O, Jørgensen P, Olsen J (1995) Chem Phys Lett 244:75

73. Pedersen TB, Koch H, Hättig C (1999) J Chem Phys 110:8318

74. London F (1937) J Phys Radium 8:397

75. Helgaker T, Jørgensen P (1991) J Chem Phys 95:2595

76. Ditchfield R (1974) Mol Phys 27:789

77. Wolinski K, Hinton JF, Pulay P (1990) J Am Chem Soc 112:8251

78. Gauss J, Stanton JF (1995) J Chem Phys 103:3561

79. Bak KL, Hansen AE, Ruud K, Heglaker T, Olsen J, Jørgensen P (1995) Theor Chim Acta 90:441

80. Helgaker T, Ruud K, Bak KL, Jørgensen P, Olsen J (1994) Faraday Discuss 99:165

81. The lack of equivalence between the length- and velocity-gauge representations of the Rosenfeld tensor for truncated coupled cluster models arises because of the lack of variational optimization of the underlying molecular orbitals, and, thus the same problem will arise for perturbation theory and multireference configuration interaction models. This problem has been addressed by Pedersen and Koch, who, in Ref. [73], developed a gauge-invariant form of coupled cluster theory through the optimized coupled cluster (OCC) approach

82. Pedersen TB, Koch H, Boman L, de Meras AMJS (2004) Chem Phys Lett 393:319

83. Polavarapu PL, Chakraborty DK (1998) J Am Chem Soc 120:6160

84. Polavarapu PL, Chakraborty DK (1999) Chem Phys 240:1

85. Kondru RK, Wipf P, Beratan DN (1998) J Am Chem Soc 120:2204

86. Perry TL, Dickerson A, Kahn AA, Kondru RK, Beratan DN, Wipf P, Kelly M, Hamann MT (2001) Tetrahedron 57:1483

87. Ribe S, Kondru RK, Beratan DN, Wipf P (2000) J Am Chem Soc 122:4608

88. Goldsmith M-R, Jayasuriya N, Beratan DN, Wipf P (2003) J Am Chem Soc 125:15696

89. Kondru RK, Wipf P, Beratan DN (1998) Science 282:2247

90. Stephens PJ, Devlin FJ, Cheeseman JR, Frisch MJ, Rosini C (2002) Org Lett 4:4595

91. Polavarapu PL (2002) Angew Chem Int Ed 41:4544

92. Hecht L, Costante J, Polavarapu PL, Collet A, Barron LD (1997) Angew Chem Int Ed 36:885

93. Schreiner PR, Fokin AA, Lauenstein O, Okamoto Y, Wakita T, Rinderspacher C, Robinson GH, Vohs JK, Campana CF (2002) J Am Chem Soc 124:13348

94. Giorgio E, Viglione RG, Zanasi R, Rosini C (2004) J Am Chem Soc 126:12968

95. Norman P, Ruud K, Helgaker T (2004) J Chem Phys 120:5027

96. Wiberg KB, Vaccaro PH, Cheeseman JR (2003) J Am Chem Soc 125:1888

97. Wiberg KB, Wang YG, Vaccaro PH, Cheeseman JR, Trucks G, Frisch MJ (2004) J Phys Chem A 108:32

98. Wiberg KB, Wang Y-G, Vaccaro PH, Cheeseman JR, Luderer MR (2005) J Phys Chem A 109:3405

99. Kumata Y, Furukawa J, Fueno T (1970) Bull Chem Soc Japan 43:3920

100. Mennucci B, Tomasi J, Cammi R, Cheeseman JR, Frisch MJ, Devlin FJ, Gabriel S, Stephens PJ (2002) J Phys Chem A 106:6102

101. Christiansen O, Koch H, Jørgensen P (1998) Chem Phys Lett 243:409

102. de Meijere A, Khlebnikov AF, Kostikov RR, Kozhushkov SI, Schreiner PR, Wittkopp A, Yufit DS (1999) Angew Chem Int Ed 38:3474

103. de Meijere A, Khlebnikov AF, Kostikov RR, Kozhushkov SI, Schreiner PR, Wittkopp A, Rinderspacher C, Menzel H, Yufit DS, Howard JAK (2002) Chem Eur J 8:828

104. Koch H, de Merás AMJS, Pedersen TB (2003) J Chem Phys 118:9481

105. Pedersen TB, de Merás AMJS, Koch H (2004) J Chem Phys 120:8887

106. Müller T, Wiberg KB, Vaccaro PH (2000) J Phys Chem A 104:5959

107. Müller T, Wiberg KB, Vaccaro PH, Cheeseman JR, Frisch MJ (2002) J Opt Soc Am B 19:125

108. Giorgio E, Rosini C, Viglione RG, Zanasi R (2003) Chem Phys Lett 376:452

109. Ruud K, Zanasi R (2005) Angew Chem Int Ed Engl 44:3594

110. Ruud K, Taylor PR, Åstrand P-O (2001) Chem Phys Lett 337:217

111. Hansen AE, Bouman TD (1980) Adv Chem Phys 44:545

112. Rauk A (1998) In: Schleyer PVR (ed) Encyclopedia of computational chemistry. Wiley, New York

113. Foresman JB, Head-Gordon M, Pople JA, Frisch MJ (1992) J Phys Chem 96:135

114. Tamm I (1945) J Phys USSR 9:449

115. Dancoff SM (1950) Phys Rev 78:382

116. Pople JA (1953) Trans Faraday Soc 49:1375

117. Del Bene JE, Ditchfield R, Pople JA (1971) J Chem Phys 55:2236

118. Grimme S, Harren J, Sobanski A, Vögtle F (1998) Eur J Org Chem 1491

119. Stanton JF, Gauss J, Ishikawa N, Head-Gordon M (1995) J Chem Phys 103:4160

120. Tozer DJ, Amos RD, Handy NC, Roos BO, Serrano-Andrés L (1999) Mol Phys 97:859

121. Dreuw A, Weisman JL, Head-Gordon M (2003) J Chem Phys 119:2943

122. Tozer DJ, Handy NC (2000) Phys Chem Chem Phys 2:2117

123. Hamprecht FA, Cohen AJ, Tozer DJ, Handy NC (1998) J Chem Phys 109:6264

124. Burcl R, Amos RD, Handy NC (2002) Chem Phys Lett 355:8

125. Pecul M, Ruud K, Helgaker T (2004) Chem Phys Lett 388:110

126. Rauk A (1984) J Am Chem Soc 106:6517

127. Hansen AE, Bouman TD (1985) J Am Chem Soc 107:4828

128. Carnell M, Peyerimhoff SD, Breest A, Godderz KH, Ochmann P, Hormes J (1991) Chem Phys Lett 180:477

129. Grimme S, Peyerimhoff SD, Bartram S, Vögtle F, Breest A, Hormes J (1993) Chem Phys Lett 213:32

130. Carnell M, Grimme S, Peyerimhoff SD (1994) Chem Phys 179:385

131. Carnell M, Peyerimhoff SD (1994) Chem Phys 183:37

132. Grimme S (1996) Chem Phys Lett 259:128

133. Pulm F, Schramm J, Hormes J, Grimme S, Peyerimhoff SD (1997) Chem Phys 224:143
134. Furche F, Ahlrichs R, Wachsmann C, Weber E, Sobanski A, Vögtle F, Grimme S (2000) J Am Chem Soc 122:1717
135. Autschbach J, Ziegler T, van Gisbergen SJA, Baerends EJ (2002) J Chem Phys 116:6930
136. Autschbach J, Jorge FE, Ziegler T (2003) Inorg Chem 42:2867
137. Neugebauer J, Baerends EJ, Nooijen M, Autschbach J (2005) J Chem Phys 122:234305
138. Pecul M, Marchesan D, Ruud K, Coriani S (2005) J Chem Phys 122:024106
139. Diedrich C, Grimme S (2003) J Phys Chem A 107:2524
140. Waletzke M, Grimme S (2000) Phys Chem Chem Phys 2:2075
141. Grimme S, Waletzke M (1999) J Chem Phys 111:5645
142. Stephens PJ, McCann DM, Devlin FJ, Cheeseman JR, Frisch MJ (2004) J Am Chem Soc 126:7514
143. Stephens PJ, McCann DM, Butkus E, Stoncius S, Cheeseman JR, Frisch MJ (2004) J Org Chem 69:1948
144. Stanton JF, Bartlett RJ (1993) J Chem Phys 98:7029
145. Christiansen O, Halkier A, Koch H, Jørgensen P, Helgaker T (1998) J Chem Phys 108:2801
146. Pedersen TB, Koch H, Ruud K (1999) J Chem Phys 110:2883
147. Pedersen TB, Hansen AE (1995) Chem Phys Lett 246:1
148. Pedersen TB, Koch H (2000) J Chem Phys 112:2139
149. Yamaguchi Y, Osamura Y, Goddard JD, Schaefer HF (1994) A new dimension to quantum chemistry: analytic derivative methods in ab initio molecular electronic structure theory, No. 29 in international series of monographs on chemistry. Oxford University Press, New York
150. Wilson EB, Decius JC, Cross PC (1980) Molecular vibrational: the theory of infrared and raman vibrational spectra. Dover, New York
151. Barron LD, Buckingham AD (2001) Acc Chem Res 34:781
152. Stephens PJ (1985) J Phys Chem 89:748
153. Buckingham AD, Fowler PW, Galwas PA (1987) Chem Phys 112:1
154. Buckingham AD (1994) Faraday Discuss 99:1
155. Stephens PJ (1987) J Phys Chem 91:1712
156. Stevens RM, Pitzer RM, Lipscomb WN (1963) J Chem Phys 38:550
157. Koch H, Jensen HJAa, Jørgensen P, Helgaker T, Scuseria GE, Schaefer HF (1990) J Chem Phys 92:4924
158. Gauss J, Stanton JF (1997) Chem Phys Lett 276:70
159. Stanton JF, Gauss J (1997) In: Bartlett RJ (ed) Recent advances in coupled-cluster methods. World Scientific Publishing, Singapore, pp 49–79
160. Gauss J, Stanton JF (1995) J Chem Phys 103:3561
161. Raghavachari K, Trucks GW, Pople JA, Head-Gordon M (1989) Chem Phys Lett 157:479
162. Bartlett RJ, Watts JD, Kucharski SA, Noga J (1990) Chem. Phys. Lett. 165:513 erratum: 167:609
163. Noga J, Bartlett RJ, Urban M (1987) Chem Phys Lett 134:126
164. Lowe MA, Segal GA, Stephens PJ (1986) J Am Chem Soc 108:248
165. Lowe MA, Stephens PJ, Segal GA (1986) Chem Phys Lett 123:108
166. Amos RD, Handy NC, Jalkanen KJ, Stephens PJ (1987) Chem Phys Lett 133:21
167. Morokuma K, Sugeta H (1987) Chem Phys Lett 134:23
168. Amos RD, Handy NC, Palmieri P (1990) J Chem Phys 93:5796
169. Stephens PJ, Jalkanene KJ, Devlin FJ, Chabalowski CF (1993) J Phys Chem 97:6107
170. Stephens PJ, Chabalowski CF, Devlin FJ, Jalkanen KJ (1994) Chem Phys Lett 225:247
171. Amos RD, Jalkanen KJ, Stephens PJ (1988) J Phys Chem 92:5571
172. Yang DY, Rauk A (1992) J Chem Phys 97:6517
173. Bak KL, Jørgensen P, Helgaker T, Ruud K, Jensen HJAa (1993) J Chem Phys 98:8873
174. Bak KL, Jørgensen P, Helgaker T, Ruud K (1994) Faraday Discuss 99:121
175. Stephens PJ, Devlin FJ, Ashvar CS, Chabalowski CF, Frisch MJ (1994) Faraday Discuss 99:103
176. Cheeseman JR, Frisch MJ, Devlin FJ, Stephens PJ (1996) Chem Phys Lett 252:211
177. Bak KL, Bludský O, Jørgensen P (1995) J Chem Phys 103:10548
178. Cappelli C, Corni S, Mennucci B, Cammi R, Tomasi J (2002) J Phys Chem A 106:12331
179. He J, Petrovich A, Polavarapu PL (2004) J Phys Chem A 108:1671
180. He J, Petrovic AG, Polavarapu PL (2004) J Phys Chem A 108:20451
181. Blanch EW, Hecht L, Syme CD, Volpetti V, Lomonossoff G, Nielsen K, Barron LD (2002) J Gen Virology 83:2593
182. Blanch EW, McColl IH, Hecht L, Nielsen K, Barron LD (2004) Vib Spectrosc 35:87
183. Barron LD, Buckingham AD (1971) Mol Phys 20:1111
184. Vibrational ROA CIDs are defined as the difference in scattering intensity of right and left circularly polarized light, arbitrarily opposite to that of VCD and ECD, which make use of rotatory strengths as a difference in left and right circularly polarized light absorption
185. Barron LD, Borgaard MP, Buckingham AD (1973) J Am Chem Soc 95:603
186. Placzek G (1934) In: Marx E (ed) Handbuch der Radiologie. Akademische, Leipzig, No. 2, p 205
187. Quinet O, Champagne B, Kirtman B (2001) J Comp Chem 22:1920
188. Jayatilaka D, Maslen PE, Amos RD, Handy NC (1992) Mol Phys 75:271
189. Bose PK, Barron LD, Polavarapu PL (1989) Chem Phys Lett 155:423
190. Bose PK, Polavarapu PL, Barron LD, Hecht L (1990) J Phys Chem 94:1734
191. Polavarapu PL (1990) J Phys Chem 94:8106
192. Polavarapu PL (1993) J Phys Chem 97:1793
193. Pecul M, Rizzo A (2003) Mol Phys 101:2073
194. Dunning TH (1989) J Chem Phys 90:1007
195. Kendall RA, Dunning TH, Harrison RJ (1992) J Chem Phys 96:6796
196. Woon DE, Dunning TH (1994) J Chem Phys 100:2975
197. Zuber G, Hug W (2004) J Phys Chem A 108:2108
198. Hehre WJ, Ditchfield R, Pople JA (1972) J Chem Phys 56:2257
199. Hariharan PC, Pople JA (1973) Theor Chim Acta 28:213
200. Bouř P (1998) Chem Phys Lett 288:363
201. Bouř P (2001) J Comp Chem 22:426
202. Ruud K, Helgaker T, Bouř P (2002) J Phys Chem A 106:7448
203. Bouř P, Kapitán J, Baumruk V (2001) J Phys Chem A 105:6362
204. Jalkanen KJ, Nieminen RM, Frimand K, Bohr J, Bohr H, Wade RC, Tajkhorshid E, Suhai S (2001) Chem Phys 265:125
205. Bouř P, Sychrovský V, Maloň P, Hanzlíková J, Baumruk V, Pospíšek J, Buděšínský M (2002) J Phys Chem A 106:7321
206. Pecul M, Rizzo A, Leszczynski J (2002) J Phys Chem A 106:11008
207. Hug W (2001) Chem Phys 264:53
208. Hug W, Zuber G, de Meijere A, Khlebnikov AE, Hansen H-J (2001) Helv Chim Acta 84:1
209. Zuber G, Hug W (2004) Helv Chim Acta 87:2208